

# Multisource LiDAR Point Cloud Registration Method Based on Progressive Optimization of Triangular Mesh Similarity in Forest Environments

Zhenyang Hui<sup>1b</sup>, Lei Lin, Shuanggen Jin<sup>1b</sup>, *Member, IEEE*, Wenbo Chen, Penggen Cheng, and Yao Yevenyo Ziggah<sup>2b</sup>

**Abstract**—The registration of LiDAR point clouds across multiple platforms in forests still poses challenges, such as unstable features for alignment, limited robustness across varying forest conditions, and uncertainties in integrating point clouds obtained from diverse LiDAR platforms. To address these challenges, this study introduces a method for registering multi-source LiDAR point clouds based on progressive optimization of triangular mesh similarity. This paper first leverages several spatial geometric features for stable registration, generated based on relative distances among neighboring trees and angles between the growth direction and the vertical zenith. Subsequently, a progressive determination and optimization strategy for registration was devised to reduce sensitivity to tree positioning accuracy in different sources of LiDAR point clouds and improve the robustness of the proposed method, particularly in complex forest environments. Furthermore, a similarity matrix was constructed to facilitate point cloud data registration across different platforms. The effectiveness of the proposed method was evaluated using 14 plots in three distinct forest sites. Experimental results demonstrate that the method yields satisfactory registration performance across various combinations of point cloud sources. The average residual distance between reference and estimated coordinates using the calculated transformation matrix was found to be 0.1589 m for the 14 plots. The average rotation and translation errors were calculated as

0.0056 degrees and 0.3470 m, respectively, confirming the successful registration outcomes achieved by the proposed method. Comparative analysis against five classical registration methods revealed that the proposed method consistently outperformed its counterparts across main accuracy indicators considered.

**Index Terms**—Multiplatform light detection and ranging (LiDAR), point cloud registration, progressive optimization, similarity matrix.

## I. INTRODUCTION

**F**OREST plays a vital role in terrestrial ecosystem [1], [2]. Accurately quantifying forest structure will benefit forest inventory and monitoring, which will help for better understanding of how terrestrial ecosystem changes in response to climate change [3]. Moreover, forest structure parameters are crucial for carbon cycle analysis [4], [5], [6]. For instance, diameter at breast height (DBH) or tree height of individual trees are key factors for estimating above ground biomass [7]. Traditional forest parameters manual measuring methods generally rely on tape measure, which is obviously time-consuming and laborious [8]. Although optical remote sensing techniques provide an efficient way for capturing forest attributes, only horizontal information of forest canopies can be obtained. Alternatively, light detection and ranging (LiDAR) has proven to be a powerful tool for forest inventory due to its capacity of 3-D point clouds acquisition and the emitted laser pulses can penetrate forest canopies to capture vertical profiles of individual trees [8], [9], [10].

According to different platforms, LiDAR system can be classified as terrestrial laser scanning (TLS), airborne laser scanning (ALS), backpack laser scanning (BLS), etc. It must be admitted that different LiDAR platforms own its advantages and limitations [11]. For instance, TLS adopts a bottom-up scanning view, which helps to obtain detailed trunk information [12]. However, single-scan mode generally encounters with huge occlusion by adjacent neighboring trees, while multiscan mode needs time-consuming registration [13], [14]. Different from TLS, ALS acquires LiDAR points using a top-down way, which means the upper canopy information can be easily obtained by ALS. Nowadays, with the fast development of autonomous aerial vehicle, unmanned laser scanning (ULS) is gradually becoming a new substitute for ALS due to its lightweight and low-cost strength [11]. However, similar to ALS, ULS has difficulties for capturing the understory information because of the occlusion

Received 24 June 2025; revised 23 August 2025 and 24 September 2025; accepted 30 October 2025. Date of publication 3 November 2025; date of current version 24 November 2025. This work was supported in part by the Outstanding Young Talents Funding of Jiangxi Province under Grant 20232ACB213017, in part by the Double Thousand Plan of Jiangxi Province under Grant DHSQT42023002, in part by the National Natural Science Foundation of China under Grant 42161060 and Grant 41801325, in part by the Funding of National Key Laboratory of Uranium Resources Exploration-Mining and Nuclear Remote Sensing under Grant 2024QZ-TD-26 and Grant 2025QZ-YZZ-08-1, and in part by the Natural Science Foundation of Jiangxi Province under Grant 20242BAB25176. (*Corresponding author: Zhenyang Hui.*)

Zhenyang Hui, Lei Lin, Wenbo Chen, and Penggen Cheng are with the National Key Laboratory of Uranium Resources Exploration-Mining and Nuclear Remote Sensing, East China University of Technology, Nanchang 330013, China, also with the School of Surveying and Geoinformation Engineering, East China University of Technology, Nanchang 330013, China, and also with the Jiangxi Key Laboratory of Watershed Ecological Process and Information, East China University of Technology, Nanchang 330013, China (e-mail: huihenyang2008@ecut.edu.cn; 2022120383@ecut.edu.cn; 202260010@ecut.edu.cn; pgcheng@ecut.edu.cn).

Shuanggen Jin is with the School of Surveying and Land Information Engineering, Henan Polytechnic University, Jiaozuo 454000, China, and also with Shanghai Astronomical Observatory, Chinese Academy of Sciences, Shanghai 200030, China (e-mail: sgjin@shao.ac.cn).

Yao Yevenyo Ziggah is with the Geomatic Engineering Department, University of Mines and Technology, Tarkwa 999064, Ghana (e-mail: yziggah@umat.edu.gh).

Digital Object Identifier 10.1109/JSTARS.2025.3628445

by the canopy [15], [16]. BLS belongs to mobile LiDAR system and can acquire large-scale point clouds efficiently without multiscan registration based on the simultaneous localization and mapping (SLAM) [17]. However, the limited vertical scanning view and measurement range will lead to upper canopy information missing [14]. From all the discussion mentioned above, it can be found that using single LiDAR platform owns its limitations. By integrating point clouds from different LiDAR sources will leverage the strengths of different LiDAR systems to obtain complete point clouds, which will help to achieve a more comprehensive understanding of forest structure and dynamics [18], [19], [20].

Based on various fusion principles, the fusion methods of multisource LiDAR point clouds in forest environments can be divided into three categories: external auxiliary information-based methods, key feature points-based methods, and individual tree attribute-based methods [14], [21].

The external auxiliary information-based fusion methods primarily make use of external data such as Global Navigation Satellite System (GNSS) positioning information [22] and color images [23] to combine point clouds from different sources. For example, the utilization of Global Positioning System (GPS) enables precise alignment between laser scanners and target positions for registration. Hauglin et al. [22] introduced a technique that utilizes GPS data to quickly match and identify airborne and terrestrial LiDAR point clouds for tree measurements. Polewski et al. [19] employed GPS-IMU systems and survey control points to register unmanned aerial vehicle (UAV) and backpack LiDAR point clouds in forests. Wang et al. [24] aligned terrestrial LiDAR data with the WGS 84 projection system using GPS information before aligning UAV and terrestrial LiDAR point clouds within the same coordinate system. However, achieving accurate control points in dense canopy areas can pose a challenge, affecting registration precision.

Key feature points-based methods typically involve the use of clustering or segmentation techniques, such as Mean Shift or DBSCAN algorithms, to identify key feature points corresponding to different point clusters within multisource LiDAR point clouds. The registration of these point clouds is achieved by aligning these key feature points. Persad and Armenakis [25] proposed a key point matching framework based on 2-D height maps to address coarse registration challenges in multisource LiDAR point clouds. The utilization of 2-D height maps effectively addresses issues related to inconsistent point densities in multiplatform LiDAR data. Dai et al. [26] employed the Mean Shift algorithm to extract key points from airborne and terrestrial LiDAR data separately. Coarse registration of these key points was carried out using the Coherent Point Drift (CPD) algorithm, followed by fine registration with the Iterative Closest Point (ICP) algorithm. However, a challenge with this method is the inefficiency of the Mean Shift approach in obtaining key points, making it less suitable for processing large-scale point cloud data. Zheng and Li [27] proposed a registration and fusion method based on differences in fast point feature histograms (FPFH) features. This approach surpasses traditional algorithms such as ICP, normal distributions transform, and fast global registration in noise-heavy point cloud scenarios. Fekry et al. [11] introduced a multilevel DBSCAN algorithm to segment tree

crowns into multiple point clusters within UAV LiDAR, backpack LiDAR, and handheld LiDAR data. They identified key points by locating local density peaks in each cluster and created feature descriptors based on the distance and azimuth of these key points to the centroid of the point set. Subsequently, graph matching was employed for coarse registration followed by fine registration using the ICP algorithm. Dai et al. [16] introduced the wood response index (WRI) for extracting key points from terrestrial and UAV LiDAR data separately, followed by initial registration using WRI filtering and binary shape context descriptors optimized through the robust random sample consensus (RANSAC) method. This method proves highly efficient and unaffected by individual tree attribute extraction accuracy.

The methods based on individual tree attributes often begin with segmenting individual trees to extract details such as tree position, height, and DBH. Subsequently, the alignment of multisource LiDAR point cloud data relies on similarities in these individual tree attributes. Guan et al. [14] employed techniques including individual tree segmentation, generation of irregular triangular meshes, and matching of these triangular meshes to gradually complete the registration of multiplatform LiDAR point cloud data. In their approach, the precise positions of the trees are crucial for successful registration. Shao et al. [28] presented a fusion and registration method for integrating single-station terrestrial and mobile mapping LiDAR data. They extracted virtual feature points based on trunk centerline information and utilized a global optimization strategy to reduce cumulative errors [29]. Wu et al. [17] introduced a step-by-step minimum spanning tree (MST) matching method for merging vehicle-mounted and backpack-mounted LiDAR data, resulting in accurate registration outcomes with minimal errors. This involved constructing an MST model based on the positions of tree trunks followed by topological similarity-based matching. While this method is highly effective, it requires precise identification of tree trunk center positions to ensure accurate point cloud matching results. Ghorbani et al. [18] separately extracted tree positions from terrestrial and airborne LiDAR data, establishing local triangular networks based on 2-D tree positions for iterative alignment, ultimately completing point cloud registration. This approach assumes that larger trees are more reliably detected and filters out small trees based on DBH information during network creation.

Recent advancements in deep learning have spurred significant innovation in point cloud registration methodologies. Wang et al. [30] introduced You Only Hypothesize Once (YOHO), a novel registration framework that achieves rotation invariance through group-equivariant feature learning. This approach demonstrates enhanced robustness to variations in point density and noise levels. The method's rotational-equivariant descriptors effectively constrain the transformation search space, substantially improving registration efficiency. Qin et al. [31] presented GeoTransformer, which incorporates geometric self-attention mechanisms and feature-based cross-attention to capture geometric invariance in point cloud data. By establishing hierarchical relationships through superpoint matching, this architecture maintains rigid transformation invariance while achieving state-of-the-art accuracy, particularly in challenging low-overlap scenarios. Addressing limitations in feature

distinctiveness, Yu et al. [32] developed rotation-invariant transformer (RoITr). This approach integrates a point-pair feature-based attention mechanism at the local level with a global transformer architecture, enabling robust point cloud matching through coordinated local-global feature refinement. Liu et al. [33] proposed RegFormer, an end-to-end transformer network designed for large-scale point cloud alignment. By implementing a multilayer attention mechanism to model spatial dependencies, this framework directly predicts rigid transformations without requiring postprocessing, streamlining the registration pipeline. Jiang et al. [34] introduced a lightweight registration method that extracts multiview features to identify overlapping regions. This strategy effectively mitigates interference from nonoverlapping points, offering a computationally efficient solution for point cloud alignment. It must be admitted that deep learning-based registration methods have demonstrated remarkable efficacy in registration. However, the majority of existing approaches focus on single-platform point cloud registration scenarios, such as point clouds acquired through TLS. Furthermore, these deep learning-based registration approaches rely heavily on labeled training samples, making the annotation process extremely time-consuming.

Although many point cloud registration methods have been proposed, there are still several unresolved challenges in forest environments. First, stable features for registration are generally unavailable in forest environments. Unlike urban environments where corner points or rectangular geometric features of building roofs can serve as stable features for registering LiDAR point clouds from multiple platforms, forest environments lack suitable features for registration, especially in complex forest settings.

Second, most recently proposed multiplatform LiDAR point cloud registration methods heavily rely on the accuracy of tree positioning [18]. However, not all trees can be correctly positioned using top-down scanning LiDAR systems such as ULS due to occlusion by the canopy. Inconsistent detection of trees from different platforms such as TLS and ULS can result in incorrectly matched trees and unsatisfactory registration results.

Lastly, existing registration methods mainly focus on TLS point cloud registration and cannot be directly applied to multiplatform registration [8]. Although multiplatform LiDAR point cloud registration has become a popular research topic, most methods are tested on single pairs of platforms such as TLS and ULS registration. The application of registration methods to point clouds from different sources simultaneously, such as TLS and ULS, TLS and BLS, and BLS and ULS, remains a question.

To address these challenges, this article proposes a multi-source LiDAR point cloud registration method in forest environments based on progressive optimization of triangular meshes similarity. The key contributions of this study can be summarized as follows:

- 1) This article leverages several spatial geometric features for stable registration, generated based on relative distances among neighboring trees and angles between the growth direction and the vertical zenith. These developed

geometric features remain consistent and stable across different scales of LiDAR source point clouds, enhancing the applicability of LiDAR point cloud data registration across diverse platforms.

- 2) A progressive determination and optimization strategy for registration was devised to reduce sensitivity to tree positioning accuracy in different sources of LiDAR point clouds and improve the robustness of the proposed method, particularly in complex forest environments.
- 3) A similarity matrix was constructed to facilitate point cloud data registration across different platforms. With this matrix's assistance, point clouds from TLS and ULS, TLS and mobile laser scanning (MLS), as well as BLS and ULS can be correctly registered.

## II. METHODOLOGY

The flowchart illustrating the proposed method is presented in Fig. 1. This article focuses on the fundamental principle of determining the rotation transformation matrix by identifying corresponding triangular meshes in point clouds obtained from different LiDAR platforms. Note that the proposed method operates exclusively within local coordinate systems and does not require georeferenced data.

To achieve this, the point clouds are initially rotated along their vertical zenith direction, which is determined by calculating the median of tree growth directions. The key element in forming matching triangular meshes is the triangle pairs, which consist of three nearest trees found in both the source and target point clouds. The process of identifying matching triangles begins with constructing a spatial structure feature vector for each triangle. This feature vector facilitates the creation of a similarity matrix by comparing feature vectors from the target and source point clouds. By analyzing this matrix, similarity values for pairs of triangles in both point clouds can be calculated using a formula that considers relative distance and growth direction angle. Subsequently, triangle pairs are identified based on these calculated similarity values, ranked from highest to lowest.

Once all matched triangle pairs have been identified, the rotation transformation matrix is refined using the RANSAC algorithm to ensure accuracy. Finally, the rotation transformation matrix is computed based on the most probable triangle pairs. In summary, the multisource point cloud registration process involves three main steps: 1) Calculating spatial structure feature vectors for triangular meshes; 2) Constructing a similarity matrix for triangle pairs; and 3) Iteratively optimizing matching triangular meshes to achieve accurate registration.

### A. Calculating Spatial Structure Feature Vectors for Triangular Meshes

As previously mentioned, the fundamental unit for comparing triangular meshes is the pair of triangles. In order to identify corresponding triangles within source and target point clouds, it is necessary to first create a vector that describes the geometric attributes of each triangle. It is important that these generated features remain consistent across different point clouds obtained



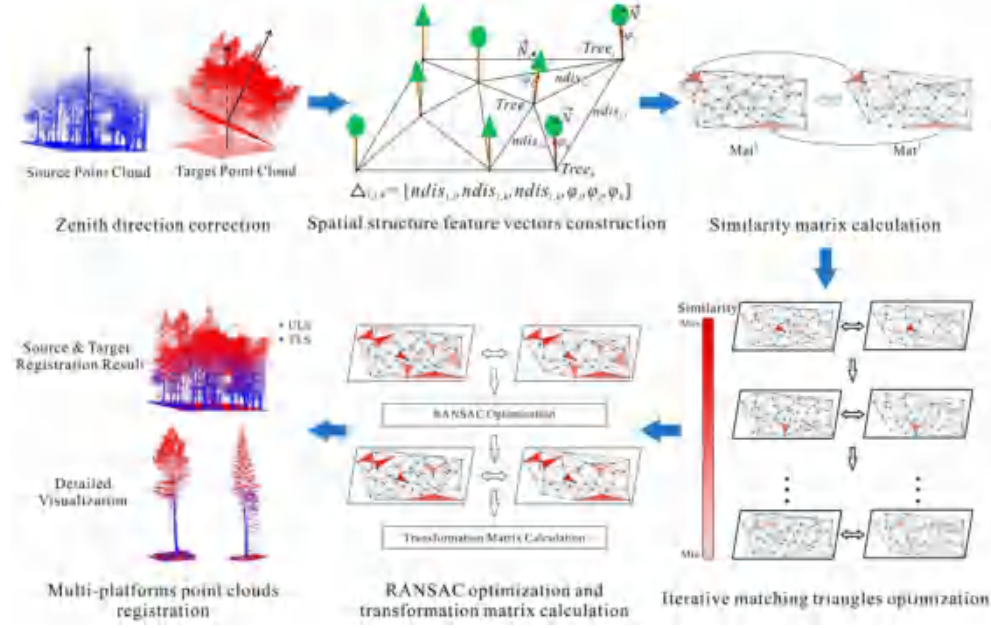


Fig. 1. Flowchart of the proposed method.

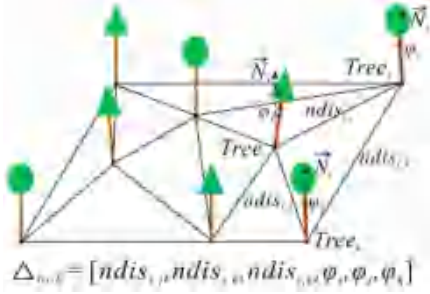


Fig. 2. Sketch map of describing the geometric features for triangular meshes generated by three nearest trees.

from varying LiDAR platforms. In this study, triangles within the point clouds are formed by the three nearest trees.

Typically, the spatial relationship between trees can be determined regardless of the LiDAR platform used to acquire the tree point clouds. As illustrated in Fig. 2, the distances between  $Tree_i$  and its neighboring trees ( $Tree_j, Tree_k$ , etc.) should exhibit similarity in both the source and target point clouds. In addition, Fig. 2 demonstrates that the growth direction of a tree ( $\vec{S}_i$ ) remains unchanged. Therefore, if the vertical zenith direction is established, it can be inferred that angles within multisource LiDAR point clouds should also demonstrate similarity. Here, “vertical zenith” refers to the gravity-aligned upward direction in the LiDAR coordinate system. It is operationally defined as the median growth direction of trees in the plot, calculated from the vector sum of individual tree orientations. This direction serves as a reference for computing growth direction angles in the following 6-D feature vector.

As illustrated in Fig. 2, the formation of triangular meshes relies on accurate detection of individual tree centers and growth orientations. To localize tree stems, vertical cross-sectional

slices are extracted from the point cloud data. For each slice, a circular model is fitted to the stem points, with the circle center determined through least-squares optimization. By tracking the trajectory of these centers across sequential slices, the primary growth axis of each tree is identified. Finally, integrating this orientation data with terrain points enables precise determination of 3-D tree positions. Note that the triangular meshes are constructed in 2-D horizontal space, where the points are projected onto a plane parallel to the ground surface. Specifically, this horizontal plane corresponds to the normalized digital terrain model (DTM) generated from the terrain points, ensuring consistent and stable triangular meshes construction for the registration process.

Consequently, this article defines a 6-D eigenvector as the feature vector for describing the geometric attributes of each triangle. This eigenvector comprises two components: relative distance  $[ndis_{ij}, ndis_{ik}, ndis_{jk}]$  and growth direction angle  $[\varphi_i, \varphi_j, \varphi_k]$  specified as follows:

$$\begin{cases} \Delta_{i,j,k} = [ndis_{ij}, ndis_{ik}, ndis_{jk}, \varphi_i, \varphi_j, \varphi_k] \\ ndis_{ij} = dis_{ij} / \max(dis_{ij}, dis_{ik}, dis_{jk}) \\ \varphi_i = \left( \widehat{\vec{S}_i, \vec{N}_i} \right) / 180 * \pi \end{cases} \quad (1)$$

where  $ndis_{ij}$  represents the relative distance between  $Tree_i$  and  $Tree_j$ .  $\varphi_i$  is the angle between its growth direction ( $\vec{S}_i$ ) and the vertical zenith direction ( $\vec{N}_i$ ).  $dis_{ij}$  is the Euclidean distance between the positions of  $Tree_i$  and  $Tree_j$ .

### B. Constructing a Similarity Matrix for Triangular Meshes

After generating the feature vectors, each triangle will be represented by a 6-D eigenvector. The triangle is formed by three

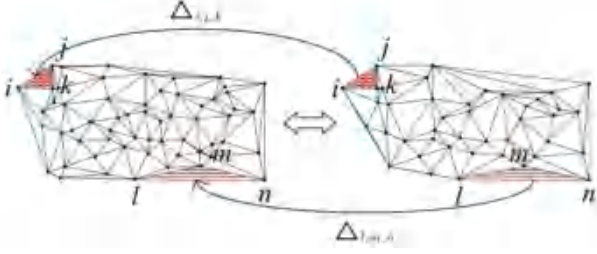


Fig. 3. Triangle pairs comparison from source and target point clouds.

nearest trees, acknowledging that different trees will have different nearest neighboring trees. For example, for  $Tree_i$  its nearest neighboring trees may be  $Tree_j$  and  $Tree_k$ . Thus, the feature vector for  $Tree_i$  is  $[ndis_{i,j}, ndis_{i,k}, ndis_{j,k}, \varphi_i, \varphi_j, \varphi_k]$ . Similarly, for  $Tree_j$ , its nearest neighboring trees may be  $Tree_k$  and  $Tree_i$ . Correspondingly, its feature vector is  $[ndis_{j,k}, ndis_{j,i}, ndis_{k,i}, \varphi_j, \varphi_k, \varphi_i]$ .

Thus, if there are  $n_1$  and  $n_2$  trees within the source and target point clouds, respectively, the source point cloud will generate a  $n_1 \times 6$  matrix ( $Mat^S$ ) as defined in (2), while the target point cloud will generate a  $n_2 \times 6$  matrix ( $Mat^T$ ).

$$Mat^S = \begin{bmatrix} ndis_{i,j}^1, ndis_{i,k}^1, ndis_{j,k}^1, \varphi_i^1, \varphi_j^1, \varphi_k^1 \\ ndis_{j,k}^2, ndis_{j,i}^2, ndis_{k,i}^2, \varphi_j^2, \varphi_k^2, \varphi_i^2 \\ \vdots \\ ndis_{o,p}^{n_1}, ndis_{o,q}^{n_1}, ndis_{p,q}^{n_1}, \varphi_o^{n_1}, \varphi_p^{n_1}, \varphi_q^{n_1} \end{bmatrix}_{n_1 \times 6} \quad (2)$$

Each tree and its nearest two trees can form a triangle and possess a feature vector. Therefore, if the source point cloud has  $n_1$  trees, there will be  $n_1$  triangles and  $n_1$  feature vectors. The same applies to the target point cloud with  $n_2$  triangles and  $n_2$  feature vectors.

To find matched triangles from the source and target point clouds, their corresponding feature vectors should be similar as depicted in Fig. 3. The triangles matching is the process of identifying corresponding triangle pairs across point clouds using similarity matrices.

This implies that the difference between these two feature vectors should be minimal. Hence, to measure the similarity of triangles from different point clouds, a similarity matrix for triangle pairs is constructed as defined in (3). Here, the matrix similarity is used to quantify structural correspondence between triangular meshes formed by neighboring trees.

$$\begin{aligned} \text{IM}_{k=1, \dots, n_1 n_2} (k, :) &= \text{Mat}^S(i, :) - \text{Mat}^T(j, :) \\ &= [\delta ndis_1^{S-T}, \delta ndis_2^{S-T}, \delta ndis_3^{S-T}, \delta \varphi_1^{S-T}, \delta \varphi_2^{S-T}, \delta \varphi_3^{S-T}]. \end{aligned} \quad (3)$$

From (3), it can be found that the similarity matrix should be a  $n_1 n_2 \times 6$  matrix since each feature vector in  $Mat^S$  must be compared to every feature vector in  $Mat^T$  to quantitatively assess the similarity among the triangles. A relative distance and growth direction angle balancing equation is formulated as (4) to evaluate this similarity.

$$\text{SV}_{k=1, \dots, n_1 n_2} (k) = \alpha \sum_{i=1,2,3} ndis_i^{S-T} + \beta \sum_{j=1,2,3} \delta \varphi_j^{S-T}. \quad (4)$$

Obviously,  $SV$  is a 1-D vector containing the calculated similarity values.  $\alpha$  and  $\beta$  are the balancing factors, which are set to 0.4 and 0.6, respectively. Note that the relative distance feature (weighted by  $\alpha$ ) exhibited robust stability across varying forest densities and LiDAR platforms, while the growth direction angle (weighted by  $\beta$ ) provided critical discriminative power for distinguishing structurally similar trees. Pre-experimental comparisons of multiple parameter combinations confirmed that these values optimally balanced stability and discriminability, ensuring consistent registration performance. Furthermore, empirical validation demonstrated that minor variations in  $\alpha$  and  $\beta$  had negligible effects on registration accuracy, justifying the use of fixed values for practical deployment.

### C. Iteratively Optimizing Matching Triangular Meshes to Achieve Accurate Registration

After constructing the similarity matrix for each triangle selected from the source and target point clouds, the similarity values for each triangle pair can be calculated using (4) and ranked from largest to smallest. Generally, the largest similarity value indicates that the two corresponding triangles in the source and target point clouds are the most likely matched triangles. This is because it signifies that the relative distances and growth direction angles among the trees forming the triangles are highly similar in both point clouds.

Subsequently, the triangle pair with the largest similarity is considered as the base for detecting other matching triangle pairs. If this base triangle pair is indeed correctly matched, other matched pairs should exhibit similar relative distances compared to the base pair. The process of detecting matched pairs is illustrated in Fig. 4. As depicted in Fig. 4(a), the triangle pairs in the source and target point clouds are color-coded similarly. The deep red color indicates higher similarity, while light red signifies lower similarity. For instance, if triangles  $A_1^S$  and  $A_1^T$  form a correct match, another pair such as  $A_2^S$  and  $A_2^T$  can be identified as a matching triangle pair if the relative distance between  $A_2^S$  and  $A_1^S$  is akin to that between  $A_2^T$  and  $A_1^T$ , as shown in Fig. 4(b). This principle guides the detection of matched triangle pairs by examining all pairs based on their similarity values, starting from the highest and progressing downward. This process is elucidated in Fig. 4(c). It is crucial to emphasize that this optimizing step is not optional but essential. Without it, the proposed method would be unable to accomplish the final registration.

Nevertheless, it must be acknowledged that there is a possibility, albeit small, that the triangle pair with the highest similarity may not be a true match. This could occur in cases where artificially planted forests have trees with structurally similar characteristics, leading to potential mismatches in triangle pairs. In such scenarios, if the pair with the highest similarity is incorrectly assumed to be the reference match, it becomes challenging to identify another pair with similar relative distances to both the reference pair and the tested pair. For example, if triangles  $A_1^S$  and  $A_1^T$  are mistakenly considered as the reference pair due to their high similarity, it may be observed that the relative distance between  $A_2^S$  and  $A_1^S$  does not align with that between  $A_2^T$  and  $A_1^T$ , as illustrated in Fig. 5. In such instances, it is necessary to

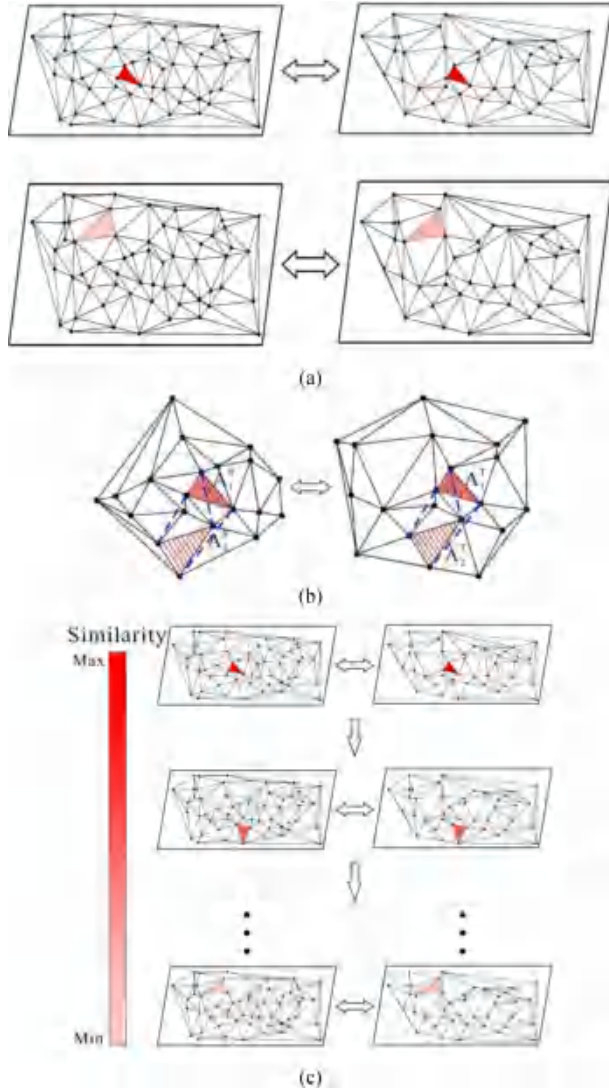


Fig. 4. Triangle pairs detection with similarity from larger to smaller. (a) Corresponding triangle pairs from source and target point clouds. The deep red color indicates higher similarity, while light red signifies lower similarity. (b) Relative distances calculation between each two matched triangle pairs. (c) Detection of matched triangle pairs according to similarity from larger to smaller.

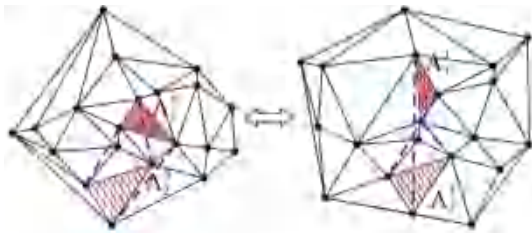


Fig. 5. Wrongly accepted triangle pair with largest similarity value.

reject the pair with the highest similarity and select the one with the second-highest value as the new reference for identifying matching pairs. Subsequent triangle pairs can then be identified following the steps outlined in Fig. 4(c).

Once all matched triangle pairs have been identified, the rotation transformation matrix is refined using the RANSAC

algorithm to ensure accuracy. Finally, the rotation transformation matrix is computed based on the most probable triangle pairs.

### III. EXPERIMENTAL RESULTS AND ANALYSIS

#### A. Experimental Datasets

To assess the effectiveness of the proposed method, this study chose three datasets from different forest sites for testing. Two of the datasets are publicly accessible, while the third dataset was recently scanned in China. The first dataset was captured at the Speulderbos Reference site in the Veluwe forest area, The Netherlands ( $N52^{\circ}15.15'$ ,  $E5^{\circ}42.00'$ ) [35]. This dataset covers around 2 ha of forest, with mature beech and oak trees on one hectare, and a mix of Douglas fir, Norway spruce, giant fir, and young beech on the other hectare. The data was collected using both ULS and TLS. The ULS data was obtained using a RIEGL RiCOPTER with VUX-1UAV laser scanner, featuring a field of scanning view of  $330^{\circ}$  and an average point density of 4059 points/m<sup>2</sup>. The TLS data was collected using a RIEGL VZ-400 laser scanner with an angular scanning resolution of  $0.06^{\circ}$  and a minimum viewing zenith angle set to  $30^{\circ}$ . Ground control points were utilized to align the ULS and TLS data. For testing purposes, six sample plots measuring  $30\text{ m} \times 30\text{ m}$  and  $60\text{ m} \times 60\text{ m}$  were utilized.

The second dataset, known as the SilviLaser 2021 Benchmark Dataset, was captured during the SilviLaser conference 2021 in Vienna [36]. It comprises circular forest plots with a radius of 25 m, showcasing various forest structures such as single-layer, multilayer, natural regeneration, and deadwood [18]. These plots contain tree species including spruce, pine, beech, and white fir. Multiple LiDAR systems including TLS and MLS were used to collect the data. The TLS data was obtained using a RIEGL VZ-400i and the MLS data was collected by GeoSlam\_ZEB\_Horizon. Point densities ranged from 200 points/m<sup>2</sup> to 200 000 points/m<sup>2</sup>. This study selected five sample plots from this dataset for testing to encompass diverse forest environments ranging from regularly grown trees with simpler structures to irregularly grown trees with higher density and complexity.

The third dataset was scanned on-site by the researchers in Lushan city, Jiangxi province, China ( $N 29^{\circ}33'4.37''$ ,  $E 115^{\circ}59'20.38''$ ). Three  $30\text{ m} \times 30\text{ m}$  sample plots were scanned using ULS and BLS, respectively. These three sample plots exhibit varying stem densities, with Cryptomeria being the predominant tree species. The ULS data was acquired using a ZENMUSE L2 laser scanner, which integrates frame LiDAR technology along with a self-developed high-accuracy IMU system and a CMOS RGB mapping camera for more precise geospatial data acquisition on DJI flight platforms. The vertical measuring accuracy of ZENMUSE L2 is 4 cm while the horizontal measuring accuracy is 5 cm. The BLS point clouds were collected using the NavVis VLX3 laser scanner, which can capture comprehensive 3-D measurements with two 32-layer LiDAR sensors combined with cutting-edge SLAM software for superior point cloud quality from a wearable device. Its



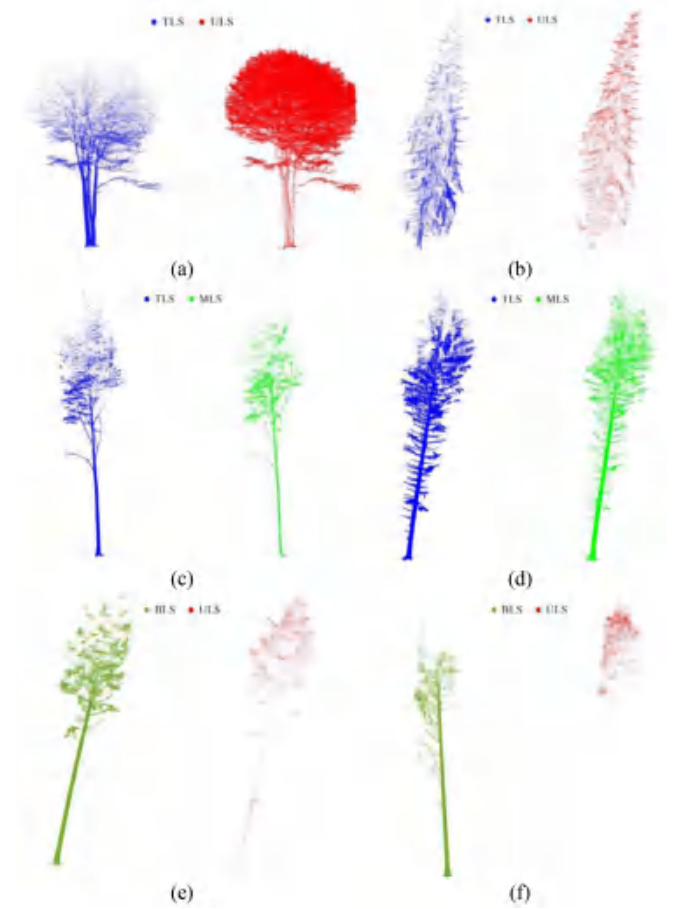


Fig. 6. Six individual tree point clouds scanned by different platforms of laser scanner from the testing sites. The blue points represent individual tree scanned by TLS. The red points represent individual tree scanned by ULS. The green points represent individual tree scanned by MLS. The olive green points represent individual tree scanned by BLS.

measuring range is up to 300 m with a capability to acquire up to 1 280 000 points/s.

In total, 14 sample plots were chosen for testing encompassing point clouds obtained through TLS, ULS, MLS, and BLS. This testing allows for assessing the performance of the proposed method in fusing point clouds from different sources. The tested tree samples from each plot are depicted in Fig. 6 where it is evident that different sources of point clouds possess distinct characteristics; for instance, TLS point clouds capture more stem details while ULS point clouds focus more on canopies. Additional details regarding the characteristics of the 14 sample plots can be found in Table I.

### B. Experimental Results

As stated in Section A, 14 plots from three forest sites were chosen for testing purposes. To visually analyze the registration results of the multisource point clouds, pairs of plots from each of the three sites were presented in Fig. 7 to demonstrate the performance of the proposed method. The profiles of each plot were specifically selected in Fig. 7 to visually showcase the registration results of the multisource point clouds. It is evident

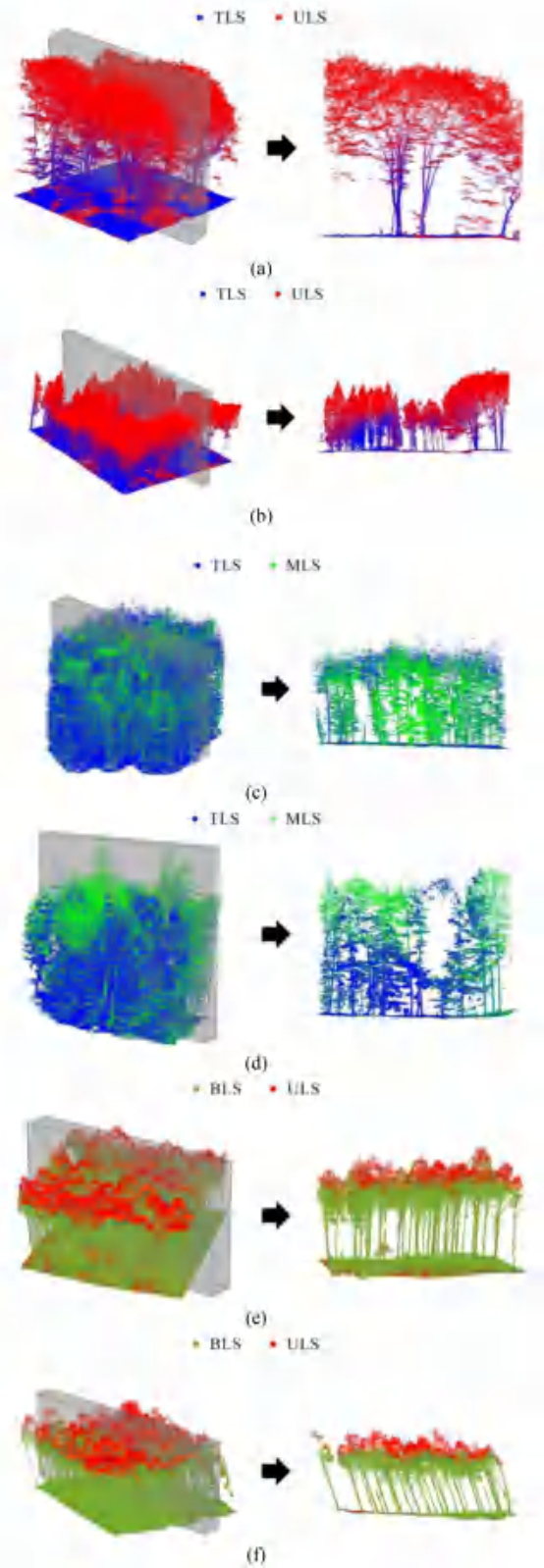


Fig. 7. Registration results for the six plots. The left sub-figures show the registration results for the plots. The transparent gray cuboid represents a cross section and the profile points are shown in the right subfigures. The blue points represent individual tree scanned by TLS. The red points represent individual tree scanned by ULS. The green points represent individual tree scanned by MLS. The olive green points represent individual tree scanned by BLS.

TABLE I  
CHARACTERISTICS OF THE 14 SAMPLE PLOTS

Sites	Plots	Laser scanners	Number of points (million point)	Tree species	Scopes	Data sources
Site1	S1-1	TLS and ULS TLS: RIEGL VZ-400 ULS:	TLS: 12.20 ULS: 4.17	Giant fir	30 m × 30 m	Brede et al. [35]
	S1-2		TLS: 14.01 ULS: 3.16	Norway spruce		
	S1-3		TLS: 8.37 ULS: 5.60	Douglas fir		
	S1-4	RIEGL VUX-1UAV	TLS: 50.24 ULS: 13.65	Young beech	60 m × 60 m	
	S1-5		TLS: 47.70 ULS: 15.27	Old beech and oak		
	S1-6		TLS: 26.49 ULS: 21.64			
Site2	S2-1	TLS and MLS	TLS: 59.27 MLS: 82.73	Spruce Pine Beech white fir	r = 25 m	Hollaus et al. [36]
	S2-2	TLS: RIEGL VZ-400i	TLS: 48.40 MLS: 106.21			
	S2-3	MLS:	TLS: 133.11 MLS: 81.93			
	S2-4	GeoSlam	TLS: 81.16 MLS: 109.48			
	S2-5	ZEB-Horizon	TLS: 81.16 MLS: 109.48			
Site3	S3-1	BLS and ULS	MLS: 49.88 ULS: 0.85	Cryptomeria	30 m × 30 m	Scanned practically
	S3-2	BLS: NavVis VLX3	MLS: 61.48 ULS: 0.96			
	S3-3	ULS: ZENMUSE L2	MLS: 51.79 ULS: 0.95			

from Fig. 7 that point clouds obtained from different LiDAR platforms exhibit distinct characteristics, as previously mentioned. For instance, TLS utilizes a bottom-up scanning mode leading to less upper canopy information, displayed in Fig. 7(a). Conversely, ULS uses a top-down scanning mode resulting in less stem information, shown in Fig. 7(b). MLS and BLS employ a similar scanning mode with a limited vertical field of view and measurement range, which enables them to capture dense trunk points but restricts canopy upper information, depicted in Fig. 7(c), (d), (e), and (f). The analysis of profiles extracted from these six plots indicates that the proposed method can effectively register multisource point clouds, such as TLS with ULS, TLS with MLS, and BLS with ULS. Following registration, the fused point clouds can address the limitations of individual data sources and provide comprehensive point cloud profiles.

Fig. 8 illustrates the detailed registration outcomes for the six trees listed in Fig. 6. In Fig. 8(a) and (b), it is evident that utilizing the proposed method enables effective registration of TLS and ULS point clouds, successfully integrating both canopy points (I and II) and branch points (III and IV). In Fig. 8(c) and (d), while TLS and MLS may be constrained by their vertical scanning views, merging MLS point clouds with TLS data compensates for occlusions observed in the TLS results, particularly noticeable in areas III and IV as shown in Fig. 8(d). In Fig. 8(e) and (f), it is clear that compared to BLS, ULS can capture more high-density canopy points in regions I and II; however, it falls short in acquiring sufficient stem points as seen in areas III and IV.

To quantitatively evaluate the performance of the proposed method, this study utilized five accuracy metrics as described in (5)–(9). The first three metrics primarily assess the residual distance of each point before and after registering the point clouds. In this research, all multisource point clouds were manually registered, meaning that the reference coordinates of each point ( $Coor_r^i$ ,  $i = 1 \dots n$ ) after registration were provided. Consequently, upon obtaining the estimated coordinates of each point ( $Coor_e^i$ ,  $i = 1 \dots n$ ) using the computed transformation matrix, the mean ( $dis_{mean}$ ), maximum ( $dis_{max}$ ), and

root mean square error ( $dis_{RMSE}$ ) of distance residual can be calculated as indicated in (5)–(7) [37]. In addition, given that the multisource point clouds were manually registered, the reference transformation matrix between the source and target point clouds was determined. This includes the reference rotation matrix ( $R_r$ ) and translation vector ( $t_r$ ). By comparing these reference values with the estimated values derived from the proposed method, the rotation error ( $E_R$ ) and the translation error ( $E_t$ ) can be computed using (8) and (9) [16].

$$dis_{mean} = \frac{\sum_{i=1}^n \|Coor_r^i - Coor_e^i\|}{n} \quad (5)$$

$$dis_{MAX} = \max_{i=1 \dots n} \|Coor_r^i - Coor_e^i\| \quad (6)$$

$$dis_{RMSE} = \sqrt{\frac{\sum_{i=1}^n \|Coor_r^i - Coor_e^i\|^2}{n}} \quad (7)$$

$$E_R = \arccos \frac{\text{tr}(R_r (R_e)^T) - 1}{2} \quad (8)$$

$$E_t = \|t_r - t_e\| \quad (9)$$

where  $Coor_r^i$  and  $Coor_e^i$  denote the reference and estimated coordinates of each point, respectively.  $\|\cdot\|$  means the distance between the referenced and estimated coordinates of each point.  $R_r$  and  $t_r$  are referenced rotation matrix and translation vector, while  $R_e$  and  $t_e$  are calculated rotation matrix and translation vector. The trace of a matrix is denoted by  $\text{tr}(\cdot)$ .

The results of accuracy metrics calculations were presented in Table II. It is evident that the average distance residual between the reference coordinates and the estimated coordinates using the computed transformation matrix for the 14 plots is 0.1589 m, indicating superior performance of the proposed method. Furthermore, the average maximum and RMSE of residual distance for the proposed method are 0.2667 m and 0.1646 m, respectively, demonstrating the method's ability to achieve precise and reliable registration results. The average rotation error and translation error are calculated as 0.0056 degrees and 0.3470 m, respectively, affirming the



TABLE II  
ACCURACY METRICS CALCULATION RESULTS FOR THE 14 PLOTS

Sites	Plots	dis <sub>mean</sub> (m)	dis <sub>max</sub> (m)	dis <sub>RMSE</sub> (m)	$E_R$ (°)	$E_t$ (m)
Site1	S1-1	0.1315	0.2206	0.1343	0.0059	0.4443
	S1-2	0.0804	0.1728	0.0853	0.0062	0.3717
	S1-3	0.1033	0.1616	0.1059	0.0033	0.4112
	S1-4	0.2506	0.5246	0.2680	0.0068	0.3795
	S1-5	0.0656	0.0880	0.0661	0.0005	0.1332
	S1-6	0.1137	0.1500	0.1153	0.0011	0.3143
Site2	S2-1	0.1129	0.2693	0.1192	0.0065	0.1319
	S2-2	0.1522	0.2451	0.1538	0.0049	0.2106
	S2-3	0.1066	0.1792	0.1083	0.0031	0.3319
	S2-4	0.1362	0.1417	0.1362	0.0014	0.2296
	S2-5	0.0620	0.1159	0.0639	0.0017	0.5330
Site3	S3-1	0.2797	0.5184	0.3008	0.0136	0.5230
	S3-2	0.3865	0.4678	0.3887	0.0077	0.2875
	S3-3	0.2437	0.4792	0.2579	0.0156	0.5565
	AVE	0.1589	0.2667	0.1646	0.0056	0.3470

satisfactory registration outcomes achieved by the proposed method.

In addition, this study computed the average accuracy metrics for each site, with comparative results displayed in Fig. 9. It is observed that the proposed method achieved similar registration outcomes in Site1 and Site2, with all five accuracy indicators exhibiting smaller values. Analysis from Table I and Fig. 6 reveals that TLS and ULS were used for point cloud acquisition in Site1, whereas TLS and MLS were utilized in Site2. By examining Fig. 6(a), (b), (c), and (d), it becomes apparent that despite using different laser scanners to capture individual tree points, the fundamental structural characteristics remain consistent, particularly for tree stems. Conversely, in contrast to Site1 and Site2, point cloud quality obtained via ULS is subpar in Site3. Examination of Fig. 6(e) and (f) reveals low point density of individual trees scanned by ULS in Site3, especially for tree stems due to canopy occlusion. Consequently, accuracy indicators for multisource point cloud registration in Site3 are a little worse than those of Site1 and Site2 as illustrated in Fig. 9.

### C. Comparison and Analysis

To objectively evaluate the performance of the proposed method, five other classical point clouds registration methods were also utilized for testing. Rusu et al. [38] proposed the FPFH point cloud registration algorithm that can efficiently describe the local geometric features of points, matches corresponding points based on these features, and computes a transformation matrix to align point clouds, achieving robust and accurate registration. Le et al. [39] introduced a robust registration method called SDRSAC. The core concept of this method involves developing a novel semidefinite-based randomized approach for robust point cloud registration without explicit correspondences. By treating the correspondence issue as a form of graph matching and using an efficient semidefinite relaxation, the authors proposed a new sampling strategy that allows the use of larger subsets for hypothesis generation. This approach combines the strengths of randomized techniques and

### Algorithm 1: Similarity Matrix Construction.

```

Input: idx_single, stempoint, high, para, dtm
1 Set 1: Cluster Filtering by Shape and Height
2 for each cluster  $i$  do
3   Extract  $P_i \leftarrow \text{stempoint}(\text{idx\_single} == i)$ ;
4   if  $|P_i| < 3$  then
5     continue
6   end
7   Compute covariance  $\Sigma_i$  and singular values  $\sigma_1 \geq \sigma_2 \geq \sigma_3$ ;
8   Compute shape metric  $\text{SoD} \leftarrow \frac{\sigma_1 - \sigma_2}{\sigma_1} + \dots$ ;
9   if  $\text{SoD} < \text{para}(1)$  or  $\text{height}(P_i) < \text{para}(2)$  then
10    continue
11  end
12 end
13 Filter remaining clusters into newstem and idx_newsingle;
14 Set 2: Estimate Base Location and Axis per Tree
15 for each cluster  $i$  in idx_newsingle do
16   Slice points vertically with height window high;
17   for each slice do
18     Fit best circle (via RANSAC + Taubin);
19     Store circle center, radius, and height
20   end
21   Remove radius outliers via  $2\sigma$  rule;
22   if too few valid circles then
23     continue
24   end
25   Estimate axis direction via SVD of circle centers;
26   if para(4) == 0 then
27     Project axis to ground height
28   else
29     Search nearest DTM point and adjust base elevation
30   end
31   if base too far from cluster then
32     continue
33   end
34   Save [base, direction] as line in Line;
35 end
36 Output: newstem, idx_newsingle, Line;

```

graph matching to swiftly filter out outliers in the sampled sets, resulting in high-quality hypotheses. Guan et al. [14] proposed a multiplatform LiDAR data fusion method based on tree locations. Five main steps were involved in their method, such as individual tree segmentation, triangulated irregular network (TIN) generation, TIN matching, etc. Among these steps, TIN matching is the core step for realizing the multiplatform point clouds registration. This article proposed a voting strategy for

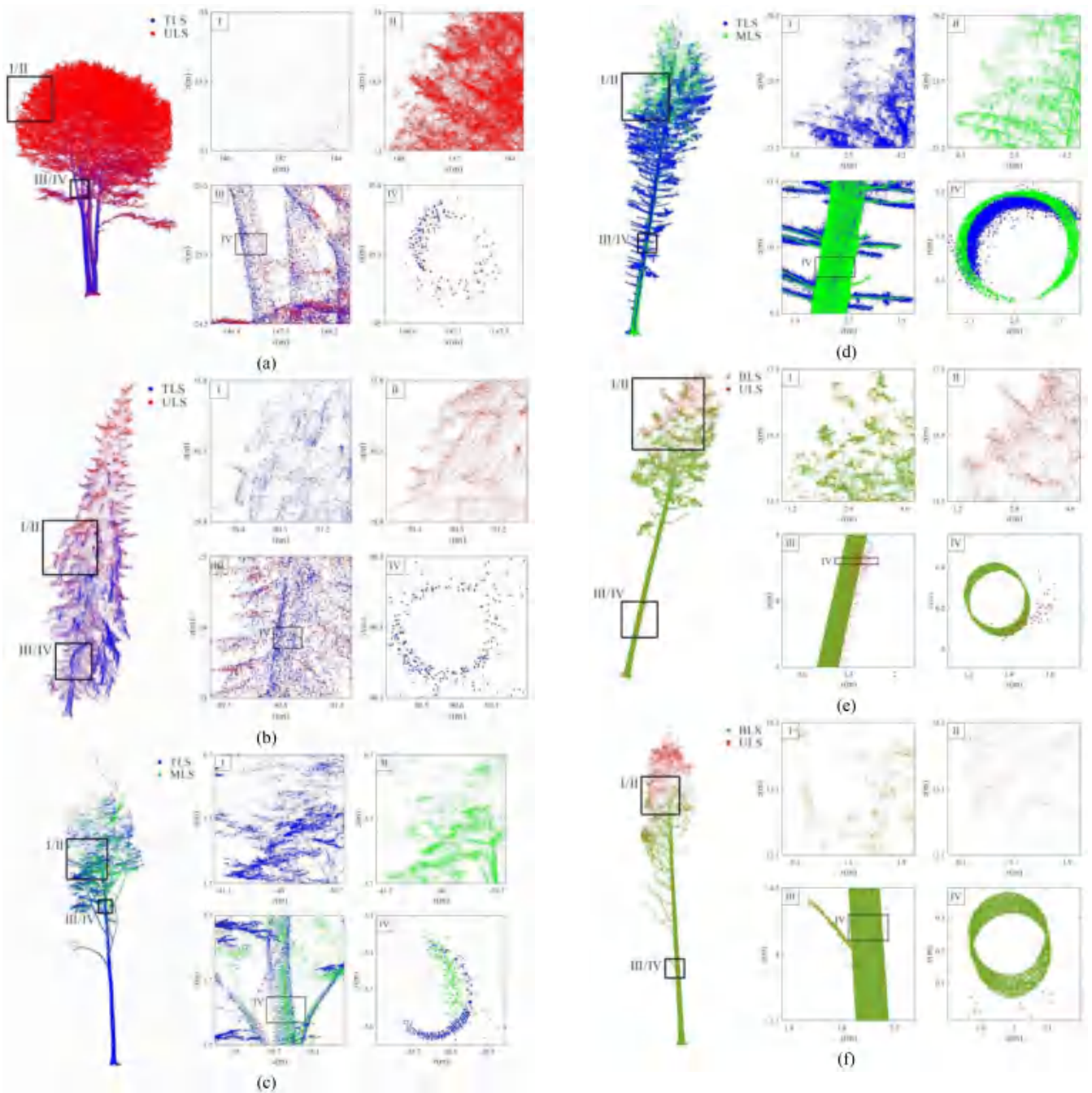


Fig. 8. (continued)

Fig. 8. Details analysis for the registration results for the six trees scanned by different platforms of laser scanner from the testing sites. The blue points represent individual tree scanned by TLS. The red points represent individual tree scanned by ULS. The green points represent individual tree scanned by MLS. The olive green points represent individual tree scanned by BLS.

fusing the backpack and UAV LiDAR data. Yang et al. [40] proposed a rapid and verifiable point cloud registration method known as TEASER. By reformulating the registration problem through a truncated least squares cost function, the algorithms are able to effectively handle many erroneous correspondences. A graph-based framework is introduced to separate scale, rotation, and translation estimation, enabling each subproblem

to be solved sequentially. Scale and translation estimation using truncated least squares are efficiently solved through an adaptive voting scheme, while rotation estimation via truncated least squares is optimized through a tight semidefinite program. In addition to conventional registration techniques, this article conducts a comparative analysis of YOHO, a state-of-the-art deep learning-based method proposed by Wang et al. [30]. This approach demonstrates superior robustness in handling variations in point density and noise levels compared to traditional methodologies.

The comparison of accuracy metrics for the 14 plots among the five methods is presented in Table III. When considering

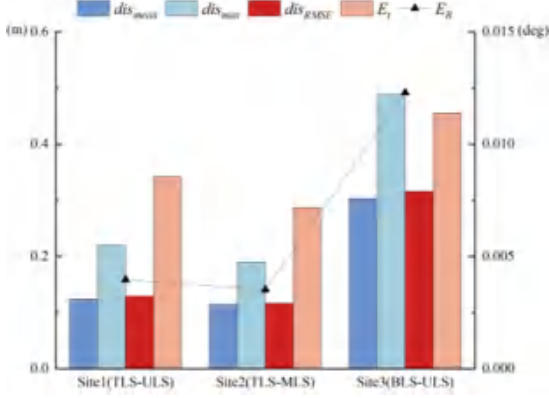


Fig. 9. Average accuracy indicators comparison for the three sites.

**Algorithm 2: Iterative Triangle Matching.**


---

**Input** :  $S_1, S_2$ : Feature point sets from source and target point clouds  
 $\tau$ : Threshold for the geometric consistency check  
 $N_{min}$ : Minimum number of required matches

- 1 **Set 1: Generate and Rank Candidate Matches** /\* Compute feature similarity scores for all pairs  $(p_i, q_j)$  and create a list  $\mathcal{L}$  ranked in descending order of score \*/
- 2  $\mathcal{L} \leftarrow \text{GenerateRankedCandidates}(S_1, S_2)$
- 3 **Set 2: Iteratively Select Geometrically Consistent Matches**  
 $\mathcal{C} \leftarrow \emptyset$  // Initialize the set of accepted matches
- 4 **for each candidate pair  $(p_i, q_j) \in \mathcal{L}$  do**
- 5   **if**  $p_i$  or  $q_j$  is already in a pair in  $\mathcal{C}$  **then**
- 6     **end** // Skip points that are already matched
- 7   **if**  $\text{IsGeometricallyConsistent}((p_i, q_j), \mathcal{C}, \tau)$  **then**
- 8      $\mathcal{C} \leftarrow \mathcal{C} \cup \{(p_i, q_j)\}$  // Accept the match if consistent
- 9   **end**
- 10 **end**
- 11 **Set 3: Estimate the Final Transformation** **if**  $|\mathcal{C}| < N_{min}$  **then**
- 12   **return failure** // Not enough matches found
- 13 **end**
- 14  $\mathcal{C}_{final} \leftarrow \mathcal{C}$
- 15  $\mathbf{T} \leftarrow \text{EstimateTransform}(\mathcal{C}_{final})$  // Compute transformation from final matches
- 16 **return**  $\mathcal{C}_{final}, \mathbf{T}$

**Output**:  $\mathcal{C}_{final}$ : The final set of robust matches  
 $\mathbf{T}$ : The rigid transformation matrix that aligns  $S_2$  to  $S_1$

---

the mean distance between referenced and estimated coordinates after registration of each point (referred to as  $\text{dis}_{\text{mean}}$ ), it is evident that the proposed method achieved significantly smaller values compared to the other methods, which recorded values tens of times larger than those of the proposed method. In addition, the proposed method consistently demonstrated stable and smaller  $\text{dis}_{\text{mean}}$  across all tested plots, whereas the  $\text{dis}_{\text{mean}}$  values obtained by other methods exhibited significant variability. For example, in plot S3-1, Le et al. [39] achieved the smallest  $\text{dis}_{\text{mean}}$  value of 0.2551 m, while in plot S1-6, the  $\text{dis}_{\text{mean}}$  value is 37.5025 m. The same findings can be concluded in terms of the other two distance accuracy indicators, such as  $\text{dis}_{\text{max}}$  and  $\text{dis}_{\text{RMSE}}$ . In terms of the rotation error ( $E_R$ ) and the translation error ( $E_t$ ), it is obvious that smaller values indicate the better registration performances. The proposed method consistently attained the smallest  $E_R$  values across all 14 tested plots, suggesting that its calculated rotation matrix ( $R_e$ ) closely approximates the reference rotation matrix. Furthermore, in

**Algorithm 3: RANSAC for Transformation Matrix Refinement.**


---

**Input**: Point sets  $A, B$ ; correspondence indices  $C$ ; adjusted points  $A$

- 1 Extract matched points:  $P_A \leftarrow A[C[:, 1], :], P_B \leftarrow B[C[:, 2], :]$ ;
- 2 Set scale  $s \leftarrow 1$ , best inlier count  $n_{\text{best}} \leftarrow 0$ ;
- 3 Initialize best model parameters;
- 4 **for**  $i \leftarrow 1$  **to**  $N_{\text{iter}}$  **do**
- 5   Randomly select 3 correspondences from  $P_A, P_B$ ;
- 6   Estimate  $(R_i, t_i) \leftarrow \text{ComputeTransform}(\cdot)$ ;
- 7   Transform all  $P_A$ :  $P'_A \leftarrow s \cdot R_i \cdot P_A^T + t_i$ ;
- 8   Compute residuals  $d_i$  between  $P'_A$  and  $P_B$ ;
- 9   Determine inliers:  $I_i = \{d_i \leq \tau\}$ ;
- 10   **if**  $|I_i| > n_{\text{best}}$  **then**
- 11     Update best model:  $R \leftarrow R_i, t \leftarrow t_i, I \leftarrow I_i, n_{\text{best}} \leftarrow |I_i|$ ;
- 12   **end**
- 13 **end**
- 14 **if**  $n_{\text{best}} < 4$  **then**
- 15   Set  $I \leftarrow$  all correspondences;
- 16 **end**
- 17 Recompute  $(R, t) \leftarrow \text{ComputeTransform}(P_A(I), P_B(I))$ ;
- 18 Compute final transformed points:  $A' \leftarrow s \cdot R \cdot A^T + t$ ;
- 19 **Output**: Rotation  $R$ , translation  $t$ , transformed points  $A'$ ;

---

terms of translation error ( $E_t$ ), results from Table III reveal that the proposed method consistently yielded smaller values for all 14 plots, outperforming the other methods in this regard. In summary, based on these observations, it can be concluded that the proposed method delivers satisfactory registration outcomes while maintaining robustness and superior performance compared to alternative methods.

Table IV presents the registration outcomes for the 14 plots using six different methods. It is observed that in the first six plots, the registration results for tree points scanned by TLS and ULS are displayed. Notably, Le et al. [39] and Yang et al. [40] exhibited the poorest registration performance in this set. The alignment of multisource point clouds showed discrepancies, with some even being in opposite directions. Rusu et al. [38] demonstrated improved registration performance for TLS and ULS point clouds, although not as precise as the proposed method.

For plots from S2-1 to S2-5, these five plots represent tree points scanned by TLS and MLS. It was noted that Le et al. [39] achieved superior performance in registering TLS and MLS point clouds compared to TLS and ULS registration. Guan et al. [14] yielded inferior results in TLS and MLS point cloud registration, while Yang et al. [40] still had the poorest performance. Compared with these traditional registration methods, the deep learning based method by Wang et al. [30] achieved better registration performance. Comparatively, the proposed method exhibited notably better registration accuracy compared to the other four methods.

The last three plots indicated the registration outcomes for BLS and ULS point clouds. It was found that Guan et al. [14], Yang et al. [40] and Wang et al. [30] had the weakest results in BLS and ULS point cloud registration, whereas Le et al. [39] achieved significantly better performance in this regard. Overall, the proposed method consistently demonstrated superior performance compared to the other methods.

Fig. 10 illustrates the comparison of registration profiles among various methods for aligning TLS and ULS point clouds. In comparison to the reference registration result shown in



TABLE III  
COMPARISON OF ACCURACY INDICATORS FOR THE 14 PLOTS AMONG THE SIX METHODS. THE BOLD FONTS REPRESENT THE SMALLEST VALUE

Plots	Methods	dis <sub>mean</sub> (m)	dis <sub>max</sub> (m)	dis <sub>RMSE</sub> (m)	$E_R$ (°)	$E_t$ (m)
S1-1	Rusu et al. [38]	1.0884	2.4860	1.1887	0.0911	6.2160
	Le et al. [39]	22.0075	49.9744	23.8813	3.0309	63.7841
	Guan et al. [14]	14.6498	45.5382	16.8050	1.5716	145.9199
	Yang et al. [40]	18.4689	44.5060	20.8214	1.9047	76.9058
	Wang et al. [30]	7.0548	15.2171	7.5901	0.2209	<b>0.2846</b>
	Proposed Method	<b>0.1315</b>	<b>0.2206</b>	<b>0.1343</b>	<b>0.0059</b>	0.4443
S1-2	Rusu et al. [38]	17.7199	35.8406	19.1336	1.5627	135.2477
	Le et al. [39]	23.3360	42.8300	24.6384	2.9846	81.0514
	Guan et al. [14]	8.1517	14.0143	8.5445	0.3189	26.0479
	Yang et al. [40]	30.3799	57.5765	31.6487	2.9095	84.9293
	Wang et al. [30]	25.1442	49.0471	25.9761	0.2440	0.3771
	Proposed Method	<b>0.0804</b>	<b>0.1728</b>	<b>0.0853</b>	<b>0.0062</b>	<b>0.3717</b>
S1-3	Rusu et al. [38]	20.3892	37.9836	21.7496	2.1476	258.5885
	Le et al. [39]	25.4038	42.8406	26.2827	3.1072	103.8912
	Guan et al. [14]	24.2518	51.3661	26.1498	2.9276	299.3980
	Yang et al. [40]	16.0693	29.9959	17.1401	1.2873	125.5128
	Wang et al. [30]	21.0023	52.0085	23.0692	0.0721	<b>0.0687</b>
	Proposed Method	<b>0.1033</b>	<b>0.1616</b>	<b>0.1059</b>	<b>0.0033</b>	0.4112
S1-4	Rusu et al. [38]	44.3199	93.3926	47.9994	2.8240	140.2170
	Le et al. [39]	34.3485	89.7093	38.1612	3.0705	115.4438
	Guan et al. [14]	6.8018	14.4195	7.3097	0.2746	13.7742
	Yang et al. [40]	52.5463	116.7466	57.9729	2.9601	122.4467
	Wang et al. [30]	14.0447	28.9048	14.9110	0.0920	<b>0.1632</b>
	Proposed Method	<b>0.2506</b>	<b>0.5246</b>	<b>0.268</b>	<b>0.0068</b>	0.3795
S1-5	Rusu et al. [38]	6.1138	13.5785	6.6374	0.2646	36.1619
	Le et al. [39]	34.2508	83.6287	37.8545	3.1008	95.5625
	Guan et al. [14]	5.9834	14.2353	6.6112	0.2572	36.2822
	Yang et al. [40]	129.4246	195.1956	132.7127	2.3084	178.5433
	Wang et al. [30]	11.2362	25.2693	12.0883	0.1232	0.1558
	Proposed Method	<b>0.0656</b>	<b>0.088</b>	<b>0.0661</b>	<b>0.0005</b>	<b>0.1332</b>
S1-6	Rusu et al. [38]	9.0288	18.3455	9.7344	0.3815	70.7773
	Le et al. [39]	37.5025	73.5147	40.1323	2.8600	38.7264
	Guan et al. [14]	6.1921	10.9845	6.5580	0.2454	43.6241
	Yang et al. [40]	20.5867	40.4956	21.6985	0.6458	116.9172
	Wang et al. [30]	26.1458	54.9088	27.9292	0.1636	0.2284
	Proposed Method	<b>0.1137</b>	<b>0.15</b>	<b>0.1153</b>	<b>0.0011</b>	<b>0.3143</b>
S2-1	Rusu et al. [38]	11.2408	31.7183	12.8193	1.2847	30.7431
	Le et al. [39]	15.2214	40.1171	16.9700	1.6359	45.9333
	Guan et al. [14]	2.9203	8.5348	3.1942	0.3334	6.9622
	Yang et al. [40]	22.1999	54.0666	23.7125	2.5675	14.9383
	Wang et al. [30]	8.7464	45.3782	10.7822	0.0779	4.1484
	Proposed Method	<b>0.1129</b>	<b>0.2693</b>	<b>0.1192</b>	<b>0.0065</b>	<b>0.1319</b>

Fig. 10(b), it is evident that Rusu et al. [38] and Wang et al. [30] achieved a satisfactory registration outcome. The ground points from both TLS and ULS scans are well-aligned, but discrepancies can be observed in the positions of tree stems between the two sources. Notably, the registration direction by Le et al. [39] is completely opposite, as depicted in Fig. 10(d). Furthermore, Fig. 10(e) and (f) reveal rotation errors in the registration results. Conversely, Fig. 10(h) displays the registration outcome using the proposed method, demonstrating successful alignment of tree stems from the distinct point sources and retaining detailed information on tree stems while incorporating rich foliage points.

Fig. 11 presents a comparison of registration profiles for TLS and MLS point clouds registration methods. Comparing with the reference result showcased in Fig. 11(b), it is noticeable that rotation errors are minimized in the registered outcomes

obtained by Rusu et al. [38], Le et al. [39] and Wang et al. [30]. Moreover, although ground points from TLS and MLS align well as illustrated in Fig. 11(c), (d) and (g), deviations are observed in tree stem positions sourced from differing origins. The registrations conducted by Guan et al. [14] and Yang et al. [40] exhibit apparent rotation errors, depicted in Fig. 11(e) and (f). Notably, the proposed method performs notably better than the other four methods, ensuring detailed branch information acquisition despite potential self-occlusion challenges.

In Fig. 12 a comparison of registration profiles for BLS and ULS point cloud registrations is presented. As evidenced in Fig. 12(b), BLS captures detailed tree points beneath the canopy, while ULS provides upper canopy information not attainable by BLS alone. Registration outcomes by Rusu et al. [38] and Guan et al. [14] display evident translation errors as shown in Fig. 12(c) and (e), whereas registrations by Le et al. [39] and

TABLE III  
(CONTINUED.)

Plots	Methods	$\text{dis}_{\text{mean}}$ (m)	$\text{dis}_{\text{max}}$ (m)	$\text{dis}_{\text{RMSE}}$ (m)	$E_R$ (°)	$E_t$ (m)
S2-2	Rusu et al. [38]	14.6572	33.6386	15.8588	1.0300	61.0651
	Le et al. [39]	18.6230	48.1937	21.1393	2.6828	111.5276
	Guan et al. [14]	13.2676	56.0707	16.5518	1.5855	10.1598
	Yang et al. [40]	24.5709	54.6413	25.3964	2.4081	20.8312
	Wang et al. [30]	9.6301	45.2664	11.8274	0.2704	4.4729
	Proposed Method	<b>0.1522</b>	<b>0.2451</b>	<b>0.1538</b>	<b>0.0049</b>	<b>0.2106</b>
S2-3	Rusu et al. [38]	2.1037	5.8724	2.3711	0.1998	15.6683
	Le et al. [39]	15.1240	48.3987	17.7006	2.2732	134.5069
	Guan et al. [14]	2.8779	6.8804	3.0121	0.1696	8.3634
	Yang et al. [40]	30.8361	70.3296	32.5329	3.0546	161.7665
	Wang et al. [30]	8.7560	46.1572	10.7236	0.4442	4.5297
	Proposed Method	<b>0.1066</b>	<b>0.1792</b>	<b>0.1083</b>	<b>0.0031</b>	<b>0.3319</b>
S2-4	Rusu et al. [38]	10.1599	27.8859	11.4854	1.0613	131.3049
	Le et al. [39]	8.3977	24.2858	9.5034	0.8185	109.2487
	Guan et al. [14]	1.9216	5.5874	2.1030	0.1685	5.8966
	Yang et al. [40]	17.3183	28.6864	17.4958	0.5356	69.6642
	Wang et al. [30]	9.5111	48.9831	11.5595	0.0861	4.8975
	Proposed Method	<b>0.1362</b>	<b>0.1417</b>	<b>0.1362</b>	<b>0.0014</b>	<b>0.2296</b>
S2-5	Rusu et al. [38]	12.1786	27.7258	13.1569	0.9376	1192.9058
	Le et al. [39]	14.6937	32.6746	15.7393	1.2051	1498.1100
	Guan et al. [14]	7.3604	13.3793	7.4901	0.1937	211.4428
	Yang et al. [40]	30.3648	69.8599	33.2140	3.1258	2631.2212
	Wang et al. [30]	12.5681	52.8825	15.4163	0.1973	3.6047
	Proposed Method	<b>0.0620</b>	<b>0.1159</b>	<b>0.0639</b>	<b>0.0017</b>	<b>0.5330</b>
S3-1	Rusu et al. [38]	5.3113	8.8586	5.5721	0.1909	9.1002
	Le et al. [39]	<b>0.2551</b>	<b>0.4987</b>	<b>0.2746</b>	0.0186	<b>0.3260</b>
	Guan et al. [14]	25.8029	51.9985	29.0217	1.5710	26.0026
	Yang et al. [40]	29.0002	60.9709	31.2477	2.7460	31.0848
	Wang et al. [30]	11.4742	20.0107	12.1183	0.7218	0.4455
	Proposed Method	0.2797	0.5184	0.3008	<b>0.0136</b>	0.5230
S3-2	Rusu et al. [38]	20.6045	53.2421	22.5064	2.0161	84.9582
	Le et al. [39]	1.3863	2.6596	1.4786	0.0661	2.5928
	Guan et al. [14]	15.9850	44.5993	17.5135	1.5950	78.7331
	Yang et al. [40]	15.4210	38.5111	16.7810	1.5423	69.8211
	Wang et al. [30]	22.2971	50.5292	23.9773	0.7154	0.5114
	Proposed Method	<b>0.3865</b>	<b>0.4678</b>	<b>0.3887</b>	<b>0.0077</b>	<b>0.2875</b>
S3-3	Rusu et al. [38]	3.7968	4.7991	3.8272	0.0564	6.0274
	Le et al. [39]	1.3593	2.8262	1.4753	0.0849	1.0586
	Guan et al. [14]	24.8071	66.2841	28.1960	1.5758	99.2052
	Yang et al. [40]	26.8625	53.4721	28.4855	2.6010	64.8482
	Wang et al. [30]	13.1110	22.4256	13.7431	0.5386	<b>0.4271</b>
	Proposed Method	<b>0.2437</b>	<b>0.4792</b>	<b>0.2579</b>	<b>0.0156</b>	0.5565

Yang et al. [40] show clear rotation errors instead. Although Wang et al. [30] achieves better the registration result, there are still registration errors compared with the referenced registration result shown in Fig. 12(b). Conversely, the proposed method showcased in Fig. 12(h) closely aligns with the reference result displayed in Fig. 12(b), enabling acquisition of both upper canopy information and detailed stem points beneath the foliage postregistration.

Tables V–IX display comparisons of average accuracy indicators among the six methods across three sites. It is evident that, regardless of the accuracy indicator used, the proposed method consistently outperforms the other four methods. The distance indicators, including  $\text{dis}_{\text{mean}}$ ,  $\text{dis}_{\text{max}}$ , and  $\text{dis}_{\text{RMSE}}$ , primarily indicate deviations between reference coordinates and postregistration coordinates. The proposed method consistently achieved the smallest values for registration of different point

cloud sources, such as TLS to ULS, TLS to MLS, and BLS to ULS.

Regarding  $E_R$ , it is notable that the largest  $E_R$  value of the proposed method is  $0.0123^\circ$  in Site3, whereas the smallest corresponding value among the other five methods is  $0.0565^\circ$ , approximately five times higher than that of the proposed method. In Site1 and Site2, the performance of the other five methods lags significantly behind that of the proposed method. In addition, when considering  $E_t$  values, it is apparent that they are several times higher than those of the proposed method, particularly for Site1 and Site2.

In conclusion, it can be inferred that irrespective of the point cloud sources selected for registration (TLS-ULS, TLS-MLS, or BLS-ULS), the proposed method consistently surpasses alternative methods in terms of accuracy indicators across all three sites.

TABLE IV  
REGISTRATION RESULTS FOR ALL THE 14 PLOTS AMONG DIFFERENT METHODS. BLUE POINTS REPRESENT INDIVIDUAL TREE SCANNED BY TLS. RED POINTS REPRESENT INDIVIDUAL TREE SCANNED BY ULS. GREEN POINTS REPRESENT INDIVIDUAL TREE SCANNED BY MLS. OLIVE GREEN POINTS REPRESENT INDIVIDUAL TREE SCANNED BY BLS


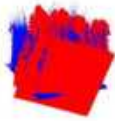
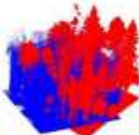

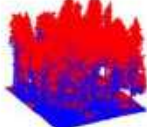
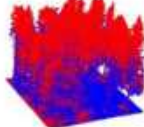
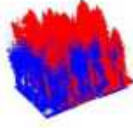
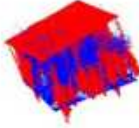
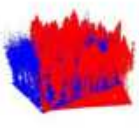

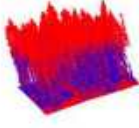
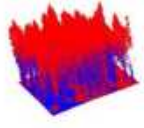

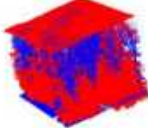
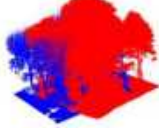

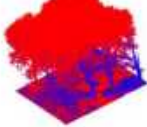
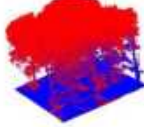
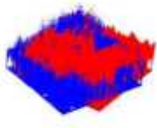
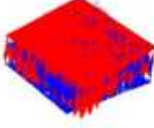
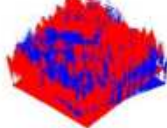


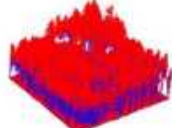
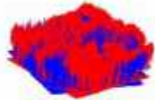

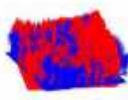

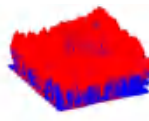
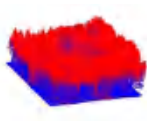
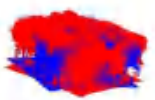





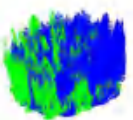
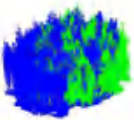
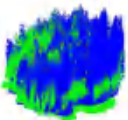
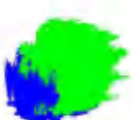
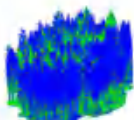
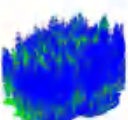
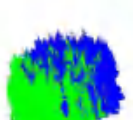
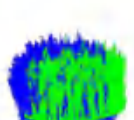
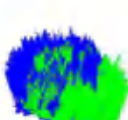

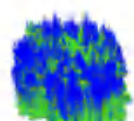
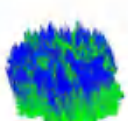
Plots	Rusu et al. [38]	Le et al. [39]	Guan et al. [14]
S1-1			
	Yang et al. [40]	Wang et al. [30]	The Proposed Method
			
S1-2			
	Yang et al. [40]	Wang et al. [30]	The Proposed Method
			
S1-3			
	Yang et al. [40]	Wang et al. [30]	The Proposed Method
			
S1-4			
	Yang et al. [40]	Wang et al. [30]	The Proposed Method
			
	Rusu et al. [38]	Le et al. [39]	Guan et al. [14]



TABLE IV  
(CONTINUED.)

S1-5			
	Yang et al. [40]	Wang et al. [30]	The Proposed Method
			
	Rusu et al. [38]	Le et al. [39]	Guan et al. [14]
S1-6			
	Yang et al. [40]	Wang et al. [30]	The Proposed Method
			
	Rusu et al. [38]	Le et al. [39]	Guan et al. [14]
S2-1			
	Yang et al. [40]	Wang et al. [30]	The Proposed Method
			
	Rusu et al. [38]	Le et al. [39]	Guan et al. [14]
S2-2			
	Yang et al. [40]	Wang et al. [30]	The Proposed Method
			
	Rusu et al. [38]	Le et al. [39]	Guan et al. [14]

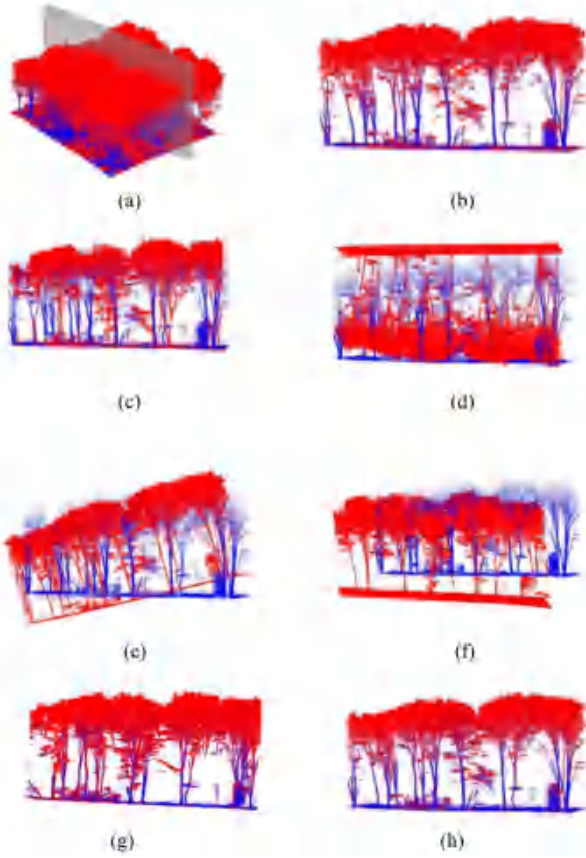


Fig. 10. Registration profiles comparison among the methods for TLS and ULS point clouds registration. The blue points represent individual tree scanned by TLS. The red points represent individual tree scanned by ULS. (a) Reference registration results for TLS and ULS point clouds. The transparent gray cuboid represents a cross section. (b) Reference registration profile points. (c) Profile points obtained by Rusu et al. [38]. (d) Profile points obtained by Le et al. [39]. (e) Profile points obtained by Guan et al. [14]. (f) Profile points obtained by Yang et al. [40]. (g) Profile points obtained by Wang et al. [30]. (h) Profile points obtained by the proposed method.

#### IV. DISCUSSION

##### A. Extreme Scenarios Analysis

While the proposed method demonstrates robust performance in multisource LiDAR point cloud registration, it inherently faces two critical limitations when applied to dense forests or young/small trees with indistinct growth direction vectors.

Fig. 13(a) illustrates point clouds acquired in a dense forest environment. Notably, individual trees cannot be properly delineated, and tree stems remain undetectable. This observation is further validated by the profile analysis in Fig. 13(b). Given that the method requires precise tree localization to derive geometric features (e.g., relative distances between neighboring trees), its effectiveness diminishes in dense forests. This issue is particularly pronounced for point clouds collected using top-down scanning systems such as ULS, where heavy canopy occlusion prevents reliable stem identification. Consequently, the foundational requirement for accurate feature computation cannot be fulfilled, leading to unsuccessful registration.

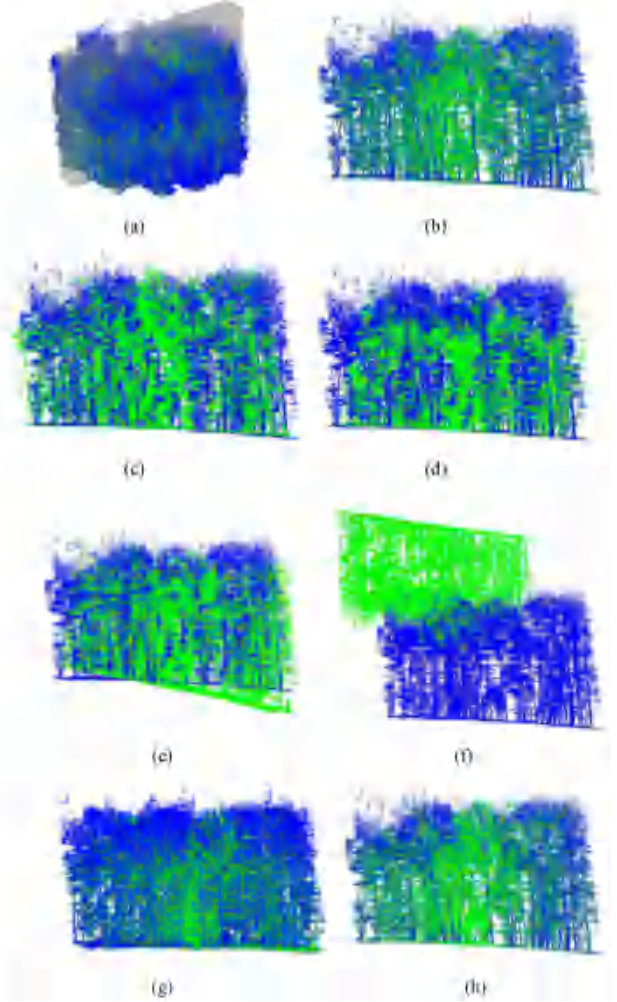


Fig. 11. Registration profiles comparison among the methods for TLS and MLS point clouds registration. The blue points represent individual tree scanned by TLS. The green points represent individual tree scanned by MLS. (a) Reference registration results for TLS and MLS point clouds. The transparent gray cuboid represents a cross section. (b) Reference registration profile points. (c) Profile points obtained by Rusu et al. [38]. (d) Profile points obtained by Le et al. [39]. (e) Profile points obtained by Guan et al. [14]. (f) Profile points obtained by Yang et al. [40]. (g) Profile points obtained by Wang et al. [30]. (h) Profile points obtained by the proposed method.

Another challenging scenario occurs in forests dominated by young/small trees, as shown in Fig. 13(c). Profile analysis in Fig. 13(d) reveals that these trees lack well-defined growth direction vectors. Since the method depends on these vectors to calculate geometric features, the absence of clear orientation cues for individual trees undermines the formation of a registration basis. Without this critical information, the algorithm fails to establish valid correspondences between point clouds, resulting in registration failure for young/small tree stands.

These findings align with experimental results from Site 3, where ULS-derived stem point clouds exhibited significantly reduced density due to canopy occlusion. This degradation directly impairs feature extraction and registration accuracy. Collectively, these limitations indicate that the method may fail

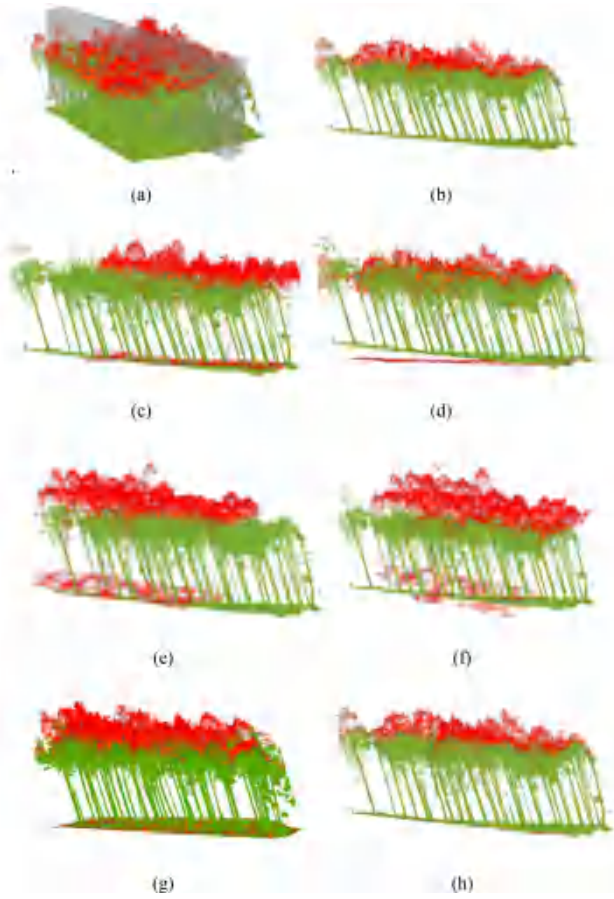


Fig. 12. Registration profiles comparison among the methods for BLS and ULS point clouds registration. The olive green points represent individual tree scanned by BLS. The red points represent individual tree scanned by ULS. (a) Reference registration results for BLS and ULS point clouds. The transparent gray cuboid represents a cross section. (b) Reference registration profile points. (c) Profile points obtained by Rusu et al. [38]. (d) Profile points obtained by Le et al. [39]. (e) Profile points obtained by Guan et al. [14]. (f) Profile points obtained by Yang et al. [40]. (g) Profile points obtained by Wang et al. [30]. (h) Profile points obtained by the proposed method.

in dense forests with severely compromised trunk visibility or in stands where trees lack distinct growth directions.

### B. Time Complexity Analysis for the Computationally Intensive Operations

This article identifies three computationally intensive operations: Similarity matrix construction, iterative triangle matching optimization, and RANSAC algorithm for transformation matrix refinement. To analyze the efficiency of the proposed method, pseudocodes for these three operations are provided.

1) *Similarity Matrix Construction (Algorithm 1)*: Algorithm 1 constructs the similarity matrix through two sequential for-loops. The first loop detects main tree stems using shape metrics and height thresholds. A computationally intensive step involves building covariance matrices for shape characterization via SVD decomposition. The number of iterations depends on detected clusters - filtering numerous clustered points significantly increases runtime. The second loop localizes tree bases and determines growth directions using geometric features.

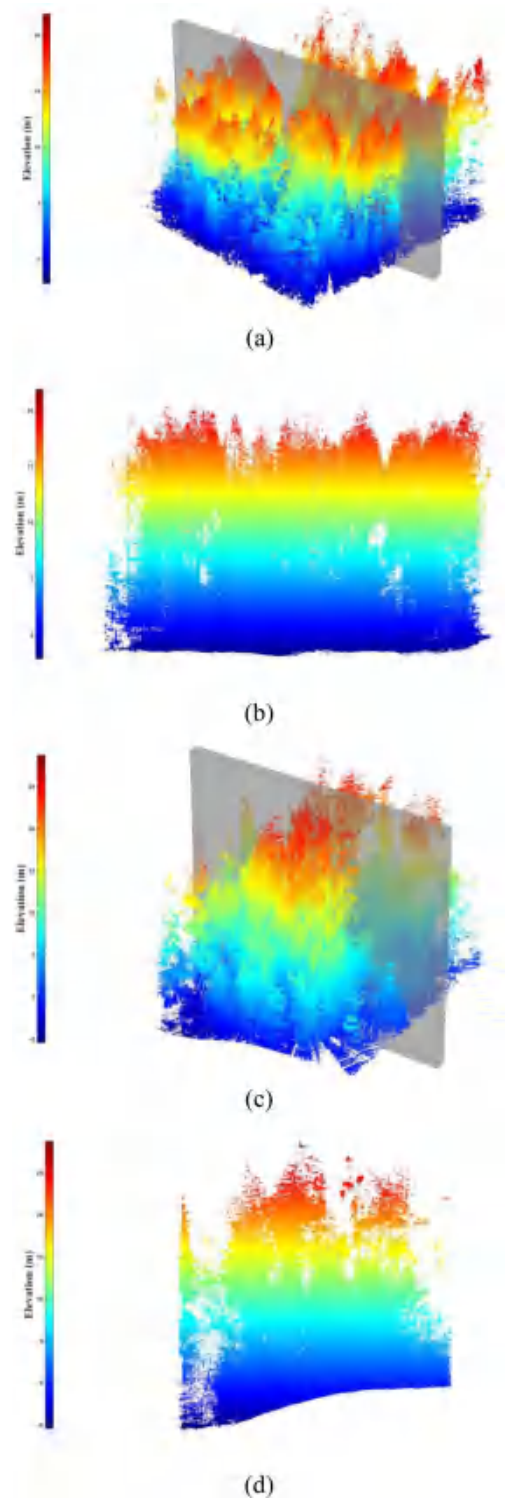


Fig. 13. Point clouds acquired in extreme scenarios. (a) and (c) Point clouds scanned in dense forest and the plot with many small young trees with indistinct growth direction vectors. The transparent gray cuboids represent cross sections. (b) and (d) Profile points are shown.

2) *Iterative Triangle Matching Optimization (Algorithm 2)*: Algorithm 2 contains three sequential steps: 1) Generating and ranking candidate matches, 2) iteratively selecting geometrically consistent matches through for-loop iterations, and 3) determining the final match set. Computational load in the first step



TABLE V  
MEAN OF DISTANCE RESIDUAL COMPARISON AMONG THE FIVE METHODS FOR THE THREE SITES. UNIT IS M

	Site1 (TLS-ULS)	Site2 (TLS-MLS)	Site3 (BLS-ULS)
Rusu et al. [38]	16.4433	10.0680	9.9042
Le et al. [39]	29.4749	14.4120	1.0002
Guan et al. [14]	11.0051	5.6696	22.1983
Yang et al. [40]	44.5793	25.0580	23.7612
Wang et al. [30]	17.4380	9.8423	15.6274
The Proposed Method	0.1242	0.1140	0.3033

TABLE VI  
MAXIMUM OF DISTANCE RESIDUAL COMPARISON AMONG THE FIVE METHODS FOR THE THREE SITES. UNIT IS M

	Site1 (TLS-ULS)	Site2 (TLS-MLS)	Site3 (BLS-ULS)
Rusu et al. [38]	33.6045	25.3682	22.2999
Le et al. [39]	63.7496	38.7340	1.9948
Guan et al. [14]	25.0930	18.0905	54.2940
Yang et al. [40]	80.7527	55.5168	50.9847
Wang et al. [30]	37.5593	47.7335	30.9885
The Proposed Method	0.2196	0.1902	0.4885

TABLE VII  
ROOT MEAN SQUARE ERROR OF DISTANCE RESIDUAL COMPARISON AMONG THE FIVE METHODS FOR THE THREE SITES. UNIT IS M

	Site1 (TLS-ULS)	Site2 (TLS-MLS)	Site3 (BLS-ULS)
Rusu et al. [38]	17.7405	11.1383	10.6352
Le et al. [39]	31.8251	16.2105	1.0762
Guan et al. [14]	11.9964	6.4702	24.9104
Yang et al. [40]	46.9991	26.4703	26.4703
Wang et al. [30]	18.5940	12.0618	16.6129
The Proposed Method	0.1292	0.1163	0.3158

TABLE VIII  
ROTATION ERROR OF DISTANCE RESIDUAL COMPARISON AMONG THE FIVE METHODS FOR THE THREE SITES. UNIT IS °

	Site1 (TLS-ULS)	Site2 (TLS-MLS)	Site3 (BLS-ULS)
Rusu et al. [38]	1.2119	0.9027	0.7545
Le et al. [39]	3.0257	1.7231	0.0565
Guan et al. [14]	0.9326	0.4901	1.5806
Yang et al. [40]	2.0026	2.3383	2.2964
Wang et al. [30]	0.1526	0.2152	0.6586
The Proposed Method	0.0040	0.0035	0.0123

scales with the number of point pairs ( $O(m^2)$ ). The second step's efficiency depends on candidate pair quantity, as each iteration verifies triangle consistency. The final step checks match sufficiency - insufficient matches result in algorithm failure.

3) *RANSAC Transformation Refinement (Algorithm 3)*: Algorithm 3 applies RANSAC to optimize transformation matrices

by minimizing residuals between pre- and post-transformation point clouds. Similar to standard RANSAC, it randomly samples 4-point correspondences to generate hypotheses. Efficiency depends on iteration count and residual thresholds. The best transformation matrix is selected based on minimal residual error.

TABLE IX  
TRANSLATION ERROR OF DISTANCE RESIDUAL COMPARISON AMONG THE FIVE  
METHODS FOR THE THREE SITES. UNIT IS M

	Site1 (TLS-ULS)	Site2 (TLS-MLS)	Site3 (BLS-ULS)
Rusu et al. [38]	107.8681	286.3374	33.3619
Le et al. [39]	83.0766	379.8653	1.3258
Guan et al. [14]	94.1744	48.5650	67.9803
Yang et al. [40]	117.5425	579.6843	55.2514
Wang et al. [30]	0.2130	4.3306	0.4613
The Proposed Method	0.3424	0.2874	0.4557

## V. CONCLUSION

Registration of LiDAR point clouds across multiple platforms in forest environments is a crucial step for forest inventory, as it allows the integration of data from various sources to overcome limitations present in single-source point cloud. To achieve a comprehensive understanding of forest structure, it is essential to register multisource point clouds. However, challenges such as unstable features during alignment, limited robustness across diverse forest conditions, and uncertainties in merging data from different LiDAR platforms need to be addressed. This study presents a method for multisource LiDAR point cloud registration based on progressive optimization of triangular mesh similarity in forest environments. A key contribution of this method is its progressive optimization strategy, aimed at improving robustness and registration accuracy across varying forest conditions. Through the optimization process, the most likely matched triangle pairs are identified progressively using a similarity matrix constructed from spatial structure feature vectors proposed in this study. The performance of the method was evaluated using 14 forest plots scanned with different LiDAR platforms including TLS, ULS, MLS, and BLS. Experimental results demonstrate significantly improved registration performance when fusing TLS point clouds with ULS point clouds and TLS point clouds with MLS point clouds. While the accuracy of registering BLS point clouds with ULS points was compromised by the quality of ULS data, the average residual distance between reference and estimated coordinates using the transformation matrix was measured at 0.1589 m for all 14 plots. The average rotation error was calculated as 0.0057°, and the translation error was 0.3470 m, affirming the successful

outcomes achieved by the proposed method. When compared to the other five alternative methods, the proposed method consistently delivers superior performance regardless of the accuracy indicators used. This article also presents a detailed comparison of profile points postregistration using various methods. It can be concluded that whether merging TLS points with ULS points, TLS points with MLS points, or BLS points with ULS points, the proposed method surpasses the performance of other methods. Postregistration, more detailed upper canopy information and abundant stem points can be obtained, especially for tree points scanned from different orientations, such as TLS scanning from bottom to top and ULS scanning from top to bottom. However, it should be acknowledged that the performance of the proposed method is inherently dependent on the quality of tree stem extraction. When processing low-quality tree stem point clouds, particularly those acquired through ULS under conditions of severe canopy occlusion, the registration accuracy may be compromised. To expand the method's applicability to challenging real-world forestry conditions while maintaining registration precision, our future research will prioritize two key directions: 1) Developing strategies to enhance the method's effectiveness when operating on low-quality tree stem point clouds; 2) Improving the method's robustness in dense forest environments where tree stem growth directions are less clearly defined or distinguishable. Furthermore, our ongoing research will also focus on: integrating deep learning-based approaches to automatically identify and weight stable geometric features in occluded environments, reducing reliance on manual feature engineering.

## REFERENCES

- [1] Y. Wang et al., "In situ biomass estimation at tree and plot levels: What did data record and what did algorithms derive from terrestrial and aerial point clouds in boreal forest," *Remote Sens. Environ.*, vol. 232, 2019, Art. no. 111309.
- [2] X. Liang et al., "International benchmarking of terrestrial laser scanning approaches for forest inventories," *ISPRS J. Photogrammetry*, vol. 144, pp. 137–179, 2018.
- [3] Y. Zhao, J. Im, Z. Zhen, and Y. Zhao, "Towards accurate individual tree parameters estimation in dense forest: Optimized coarse-to-fine algorithms for registering UAV and terrestrial LiDAR data," *Giscience Remote Sens.*, vol. 60, no. 1, 2023, Art. no. 2197281.
- [4] M. Demol et al., "Estimating forest above-ground biomass with terrestrial laser scanning: Current status and future directions," *Methods Ecol. Evol.*, vol. 13, no. 8, pp. 1628–1639, 2022.
- [5] J. G. D. Tanago et al., "Estimation of above-ground biomass of large tropical trees with terrestrial lidar," *Methods Ecol. Evol.*, vol. 9, no. 2, pp. 235–246, 2018.
- [6] G. Goldbergs, S. R. Levick, M. Lawes, and A. Edwards, "Hierarchical integration of individual tree and area-based approaches for savanna biomass uncertainty estimation from airborne lidar," *Remote Sens. Environ.*, vol. 205, pp. 141–150, 2018.
- [7] Z. Hui, S. Jin, P. Cheng, and Y. Y. Ziggah, "FGA: An allometric model for revealing the relationship between fractal geometry and AGB estimation," *IEEE Trans. Geosci. Remote Sens.*, vol. 61, 2023, Art. no. 5705712.
- [8] J. Chen, D. Zhao, Z. Zheng, C. Xu, Y. Pang, and Y. Zeng, "A clustering-based automatic registration of UAV and terrestrial lidar forest point clouds," *Comput. Electron. Agriculture*, vol. 217, 2024, Art. no. 108648.
- [9] D. Panagiotidis, A. Abdollahnejad, and M. Slavík, "A clustering-based automatic registration of UAV and terrestrial lidar forest point clouds," *Int. J. Appl. Earth Observ.*, vol. 112, 2022, Art. no. 102917.

- [10] S. Jin et al., "Lidar sheds new light on plant phenomics for plant breeding and management: Recent advances and future prospects," *ISPRS J. Photogrammetry*, vol. 171, pp. 202–223, 2021.
- [11] R. Fekry, W. Yao, L. Cao, and X. Shen, "Ground-based/UAV-LiDAR data fusion for quantitative structure modeling and tree parameter retrieval in subtropical planted forest," *Forest Ecosystems*, vol. 9, 2022, Art. no. 100065.
- [12] Z. Dong et al., "Registration of large-scale terrestrial laser scanner point clouds: A review and benchmark," *ISPRS J. Photogrammetry*, vol. 163, pp. 327–342, 2020.
- [13] C. Paris, D. Kelbe, J. Van Aardt, and L. Bruzzone, "A novel automatic method for the fusion of ALS and TLS Lidar data for robust assessment of tree crown structure," *IEEE Trans. Geosci. Remote Sens.*, vol. 55, no. 7, pp. 3679–3693, Jul. 2017.
- [14] H. Guan et al., "A novel framework to automatically fuse multiplatform lidar data in forest environments based on tree locations," *IEEE Trans. Geosci. Remote Sens.*, vol. 58, no. 3, pp. 2165–2177, Mar. 2020.
- [15] W. Zhang et al., "Automated marker-free registration of multisource forest point clouds using a coarse-to-global adjustment strategy," *Forests*, vol. 12, no. 3, 2021, Art. no. 269.
- [16] W. Dai et al., "Multisource forest point cloud registration with semantic-guided keypoints and robust ransac mechanisms," *Int. J. Appl. Earth Observ.*, vol. 115, 2022, Art. no. 103105.
- [17] B. Wu et al., "A stepwise minimum spanning tree matching method for registering vehicle-borne and backpack lidar point clouds," *IEEE Trans. Geosci. Remote Sens.*, vol. 60, 2022, Art. no. 5705713.
- [18] F. Ghorbani, C. Y. Chen, M. Hollaus, and N. Pfeifer, "A robust and automatic algorithm for Tls–Als point cloud registration in forest environments based on tree locations," *IEEE J. Sel. Top. Appl. Earth Observ. Remote Sens.*, vol. 17, pp. 4015–4035, 2024.
- [19] P. Polewski, W. Yao, L. Cao, and S. Gao, "Marker-free co-registration of UAV and backpack LiDAR point clouds in forested areas," *ISPRS J. Photogrammetry*, vol. 147, pp. 307–318, 2019.
- [20] E. Lee, Y. Kwon, C. Kim, W. Choi, and H. Sohn, "Multi-source point cloud registration for urban areas using a coarse-to-fine approach," *Giscience Remote Sens.*, vol. 61, no. 1, 2024, Art. no. 2341557.
- [21] Z. Dong, B. Yang, F. Liang, R. Huang, and S. Scherer, "Hierarchical registration of unordered Tls point clouds based on binary shape context descriptor," *ISPRS J. Photogrammetry*, vol. 144, pp. 61–79, 2018.
- [22] M. Hauglin, V. Lien, E. N. Sset, and T. Gobakken, "Geo-referencing forest field plots by co-registration of terrestrial and airborne laser scanning data," *Int. J. Remote Sens.*, vol. 35, no. 9/10, pp. 3135–3149, 2014.
- [23] B. O. Abayowa, A. Yilmaz, and R. C. Hardie, "Automatic registration of optical aerial imagery to a lidar point cloud for generation of city models," *ISPRS J. Photogrammetry*, vol. 106, pp. 68–81, Aug. 2015.
- [24] M. Wang, J. Im, Y. Zhao, and Z. Zhen, "Multi-platform lidar for non-destructive individual aboveground biomass estimation for Changbai larch (*Larix olgensis* Henry) using a hierarchical Bayesian approach," *Remote Sens.*, vol. 14, 2022, Art. no. 4361.
- [25] R. A. Persad and C. Armenakis, "Automatic co-registration of 3D multi-sensor point clouds," *ISPRS J. Photogrammetry*, vol. 130, no. 5, pp. 162–186, 2017.
- [26] W. Dai et al., "Automated fusion of forest airborne and terrestrial point clouds through canopy density analysis," *ISPRS J. Photogrammetry*, vol. 156, pp. 94–107, 2019.
- [27] L. Zheng and Z. Li, "Virtual namesake point multi-source point cloud data fusion based on FPFH feature difference," *Sensors*, vol. 21, no. 16, 2021, Art. no. 4361.
- [28] J. Shao et al., "Slam-aided forest plot mapping combining terrestrial and mobile laser scanning," *ISPRS J. Photogrammetry*, vol. 163, pp. 214–230, 2020.
- [29] Q. Liu et al., "Target-free ULS-TLS point-cloud registration for alpine forest lands," *Comput. Electron. Agriculture*, vol. 190, 2021, Art. no. 106460.
- [30] H. Wang, Y. Liu, Z. Dong, and W. Wang, "You only hypothesize once: Point cloud registration with rotation-equivariant descriptors," in *Proc. 30th ACM Int. Conf. Multimedia*, 2022, pp. 1630–1641.
- [31] Z. Qin, H. Yu, C. Wang, Y. Guo, Y. Peng, and K. Xu, "Geometric transformer for fast and robust point cloud registration," in *Proc. IEEE/CVF Conf. Comput. Vis. Pattern Recognit.*, 2022, pp. 11143–11152.
- [32] H. Yu et al., "Rotation-invariant transformer for point cloud matching," 2023, *arXiv:2303.08231*.
- [33] J. Liu, G. Wang, Z. Liu, C. Jiang, M. Pollefeys, and H. Wang, "Regformer: An efficient projection-aware transformer network for large-scale point cloud registration," in *Proc. IEEE/CVF Int. Conf. Comput. Vis.*, 2023, pp. 8451–8460.
- [34] L. Jiang, Y. Liu, Z. Dong, Y. Li, and Y. Lin, "Lightweight deep learning method for end-to-end point cloud registration," *Graph Models*, vol. 137, 2025, Art. no. 101252.
- [35] B. Brede et al., "Non-destructive tree volume estimation through quantitative structure modelling: Comparing UAV laser scanning with terrestrial LiDAR," *Remote Sens. Environ.*, vol. 233, 2019, Art. no. 111355.
- [36] M. Hollaus, "Silvilaser 2021 benchmark dataset - terrestrial challenge," in *Proc. SilviLaser Conf.*, 2021, pp. 1–364.
- [37] B. Yang, Y. Zang, Z. Dong, and R. Huang, "An automated method to register airborne and terrestrial laser scanning point clouds," *ISPRS J. Photogrammetry*, vol. 109, pp. 62–76, 2015.
- [38] B. R. Rusu, N. Blodow, and M. Beetz, "Fast point feature histograms (FPFH) for 3D registration," in *Proc. IEEE Int. Conf. Robot. Automat.*, 2009, pp. 3212–3217.
- [39] H. M. Le, T. T. Do, T. Hoang, and N. M. Cheung, "SDRSAC: Semidefinite-based Randomized Approach for Robust Point Cloud Registration without Correspondences," in *Proc. IEEE/CVF Conf. Comput. Vis. Pattern Recognit.*, 2019, pp. 124–133.
- [40] H. Yang, J. Shi, and L. Carlone, "Teaser: Fast and certifiable point cloud registration," *IEEE Trans. Robot.*, vol. 37, no. 2, pp. 314–333, Apr. 2021.



**Zhenyang Hui** was born in Kaifeng, Henan, China, in 1989. He received the B.S. degree in surveying engineering from the Henan University of Engineering, Zhengzhou, China, in 2008, and the Ph.D. degree in geodesy and survey engineering from the China University of Geosciences, Wuhan, China, in 2017. From 2017 to 2024, he was a Lecturer and Associate Professor with the School of Surveying and Geoinformation Engineering, East China University of Technology, where he is currently a Professor. He has authored more than 60 peer reviewed journal articles. His research interests include LiDAR point clouds processing, artificial intelligence, machine learning, and pattern recognition. Prof. Hui was the recipient of Jiangxi Province outstanding surveying and mapping geographic information technology young talents (2021), Jiangxi Province double thousand and plan high-level talents (2022), and Jiangxi Outstanding Youth Fund (2023).



**Lei Lin** was born in Anqing, Anhui, China in 1999. He received the B.S. degree in surveying and mapping engineering from Jiangsu Ocean University, Lianyungang, China, in 2021. He is currently working toward the master's degree in surveying and mapping engineering with East China University of Technology, Nanchang, China. His research interests focus on LiDAR point clouds processing.





**Shuanggen Jin** (Senior Member, IEEE) was born in Anhui, China, in 1974. He received the B.Sc. degree in geodesy from Wuhan University, Wuhan, China, in 1999, and the Ph.D. degree in geodesy from the University of Chinese Academy of Sciences, Beijing, China, in 2003. He is currently the Vice-President and Professor with Henan Polytechnic University, Jiaozuo, China, and also a Professor with Shanghai Astronomical Observatory, CAS, Shanghai, China. He has more than 500 papers in peer-reviewed journals and proceedings, 10 patents/software copyrights,

and 10 books/monographs with more than 9000 citations and H-index >50. His main research interests include satellite navigation, remote sensing, space geodesy, and space/planetary exploration. Prof. Jin was the recipient of one first-class and four second-class prizes of provincial awards, 100-Talent Program of CAS (2010), Fellow of IAG (2011), Fu Chengyi Youth Sci. and Tech. Award (2012), Xia Jianbai Award of Geomatics (2014), Member of Russian Academy of Natural Sciences (2017), Member of European Academy of Sciences (2018), IUGG Fellow (2019), Member of Academia Europaea (2019), Member of Turkish Academy of Sciences (2020), World Class Professor of Ministry of Education and Cultures, Indonesia (2021), Fellow of Electromagnetics Academy, USA (2021) etc. He has been the President of International Association of Planetary Sciences (IAPS) (2013–2017), President of the International Association of CPGPS (2016–2017), Chair of IUGG Union Commission on Planetary Sciences (UCPS) (2015–2023), Vice-President of the IAG Commission 2 (2015–2019), Vice-Chair of COSPAR's Panel on Satellite Dynamics (PSD) (2016–2020), Editor-in-Chief of *International Journal of Geosciences* (2010–), Associate Editor of IEEE TRANSACTIONS ON GEOSCIENCE AND REMOTE SENSING (2014–), Associate Editor of *Journal of Navigation* (2014–), Associate Editor of *Advances in Space Research* (2013–2017), Editorial Board member of GPS Solutions (2016–), *Journal of Geodynamics* (2014–), and *Planetary and Space Science* (2014–).



**Wenbo Chen** was born in 1974. He received the B.S. and M.S. degrees in forestry from Jiangxi Agricultural University (JAU), Nanchang, China, in 1996 and 1999, and the Ph.D. degree in ecology from the Graduate School of the Chinese Academy of Sciences, Beijing, China, in 2002. From 2003 to 2008, he was an Associate Professor with the School of Land Resources and Environment, JAU, progressing to a full Professor until 2016. From 2007 to 2008, he was a Visiting Scholar with Wageningen University, The Netherlands. Following this, he was a Professor

with the Center for Teaching Quality Supervision and Evaluation (CTQSEC), JAU, until 2022. He is currently a Professor with the School of Surveying, Mapping and Spatial Information Engineering, Donghua University of Science and Technology, Shanghai, China. He has authored more than 100 academic papers as either the first or corresponding author. His research interests include landscape ecology, land evaluation, land remote sensing, and information. Prof. Chen serves as a peer review expert for the National Natural Science Foundation of China and is an expert in public management disciplines evaluation for the Ministry of Education in China. In addition, he is the Vice President of the Natural Resources Assessment and Evaluation Association of Jiangxi Province and is a Member of its Expert Committee. He also serves as the Vice President of the Land Institute of Jiangxi Province, a member of the Landscape Ecology Committee of the Ecological Society of China, and sits on the Board of Directors for both the International Society of Landscape Ecology - China Chapter and the International Society of Landscape Ecology as a whole.



**Penggen Cheng** was born in Nanchang, Jiangxi, China in 1964. He received the B.S. degree in surveying engineering from the East China Institute of Geology, Fuzhou, China, in 1985, the M.S. degree in photogrammetry and remote sensing from Wuhan Technology University of Surveying and Mapping, Wuhan, China, in 1996, and the Ph.D. degree in photogrammetry and remote sensing from Wuhan University, Wuhan, in 2005. From 1985 to 2000, he was a Lecturer, Associate Professor with the Surveying Department, East China Institute of Geology. From

2008 to 2009, he was a Visiting Scholar with University of Waterloo, Canada. Since 2000, he has been a Professor with the Faculty of Geomatics, East China University of Technology. He has authored four books and more than 180 articles. His research interests include geographic information system theory and software development, 3-D data model theory and application, remote sensing geo-mapping, and urban ecological environment monitoring. Prof. Cheng was a recipient of Yexue'an Excellent Teacher Award in 2017, and a young and middle-aged expert with outstanding contributions from National Nuclear Industry Corporation of China in 1998, and an expert on special government allowances under the State Council in 2002. He is an Editor of *Geography and Geographical Information Science*.



**Yao Yevenyo Ziggah** was born in Agona Ninta, Central Region, Ghana, in 1984. He received the bachelor of science degree (Hons.) in geomatic engineering from the Kwame Nkrumah University of Science and Technology (KNUST), Kumasi, Ghana, in 2008, the master of engineering and Doctor of Philosophy degrees in geodesy and survey engineering from the China University of Geosciences (CUG), Wuhan, China, in 2013 and 2017, respectively. Since 2017, he has been a Lecturer with the Geomatic Engineering Department, University of Mines and Technology

(UMaT), Ghana. He has authored more than 45 peer reviewed journal articles. His research interests include application of artificial intelligence in engineering, 2-D/3-D coordinate transformation, height systems, gravity field modeling, and geodetic deformation modeling. Dr. Ziggah was a recipient of the UMaT staff development fund, Ghana Government Scholarship, and Chinese Government Scholarship to pursue master and doctorate degrees, and was awarded the second best paper at the Geographic Information System, Geodesy and Survey Engineering conference in 2015 at Changsha, China.